CHAPTER 3 Computer Program

3.1 Introduction

The primary objective of this project was to develop and evaluate measures to improve the energy efficiency of domestic refrigerators. This chapter describes the development of a program that allows the performance of the refrigerator to be simulated. Using a simulation program is a cost-effective method to evaluate various proposals so that only those which demonstrate the potential of enhancing the performance of the system will be considered for implementation. Hence, the computer model remains an essential and important part of this research since it provides the foundation for evaluating system options.

3.2 Basic Approach

In most domestic refrigerators, the compressors that drive the cycles are often oversized. Due to issues with the commercial availability of small compressors and the low efficiency of such units, the manufacturer of this refrigerator has decided to maintain the use of the present compressors in this refrigerator. Although the compressor capacity Under normal operating conditions (5°F for the freezer and 38°F for the refrigerator, 90°F ambient), the compressors in this refrigerator do not run beyond 45% of the time to meet the

cooling loads in their respective compartments. Owing to the cyclical nature of this operation, the entire process is transient and steady-state conditions are almost never achieved. At design conditions (5°F for the freezer and 38°F for the refrigerator, 90°F ambient), the freezer cycles on for 21 minutes while the on-cycle time for the refrigerator is 24 minutes. With such short cycle times, the system usually enters the off-cycle mode before it reaches steady-state (for the time constant of the cooling process, refer to Section 3.4.4 which shows the change in mass flow rate and power as a function of time). Even with the inherent transient behavior, it is still possible to utilize a quasi-steady simulation approach by taking time averages over the cycle to yield mean values for certain parameters. To lend more credibility for this approach, experimental data have confirmed that every cycle is repeatable and system-operating parameters do not change significantly from one cycle to another. In other words, this simulation program employs a quasi steady-state model to represent the transient processes that occur in the vapor-compression cycle operating during its run cycle. Figure 3.1 is a schematic of the vapor-compression cycle that was used to simulate both the freezer and refrigerator cycles in this unit.

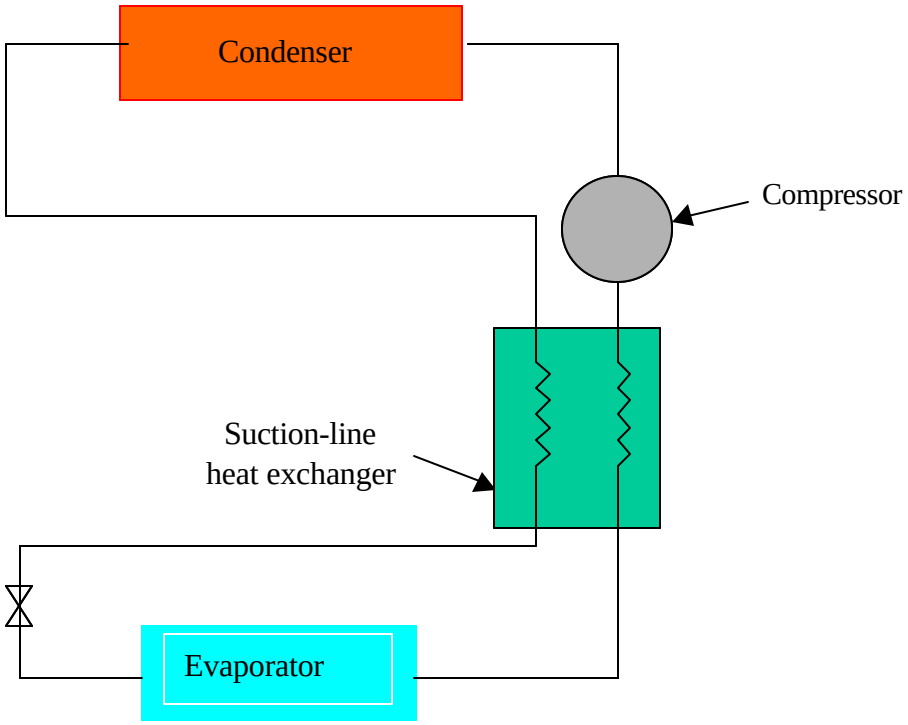

Figure 3.1 Schematic of the major components in a vapor-compression cycle.

In developing the model, an energy balance was performed on every component in the cycle. With the effects of gravity and velocity changes negligible, at steady-state, the amount of heat transferred or work done is only related to the enthalpy difference and the refrigerant mass flow entering and leaving each component, as Eqn. 3.1 shows.

$$\dot{Q} - \dot{W} = \sum_{out} \dot{m} h_{out} - \sum_{in} \dot{m} h_{in} \qquad \text{Eqn. 3.1}$$

The program, in general, consists of a collection of energy balances on components that were arranged to reflect the direction of flow in Figure 3.1. Analysis was performed using the EES software. These energy balances alone are, however, not able to

independently yield the desired outputs of the refrigeration capacity, compressor power consumption and percentage run times of the compressor. To enable the determination of these parameters, various assumptions and inputs that were specific to this refrigerator and freezer were needed.

3.3 Assumptions

In this program, two assumptions were made. The first involves the state of the refrigerant that leaves the evaporator and condenser while the second assumption is related to the cycling losses that the cycles experience.

3.3.1 Saturated Conditions at Heat Exchanger Outlets

The simulation program evaluates the enthalpies, temperatures and pressures of the refrigerant at every point in the cycle in Figure 3.1. While the enthalpy is a function of the temperature and pressure alone in the superheated and subcooled region, the quality of the refrigerant is required to define its enthalpy in the two-phase region. In this program, the refrigerant was assumed to be saturated at the exit of the evaporator and condenser. Any deviation from these assumptions would not contribute to any significant errors as most of

the heat transfer in these devices is accomplished, primarily, through the phase change of the refrigerant and not by the effects of superheat or subcooling.

3.3.2 Cycling Losses

During the normal sequence of operations, a rise in cabinet temperature a few degrees above the setpoint causes the compressor to cycle on to initiate the cooling process. The compressor ceases operation after the cabinet temperature falls a few degrees below the setpoint temperature. At the time when the compressor cycles off, the pressure is much higher in the condenser than the evaporator. To equalize this imbalance in pressure, refrigerant migrates from the condenser to the evaporator via the capillary tube and warms up the evaporator in the process. It is the warming of the evaporator and the redistribution of this off-cycle refrigerant migration that degrades the performance of the system. Besides the need for charge redistribution, the evaporator needs to be cooled before heat transfer between the air and refrigerant in the evaporator is possible. Hence, a portion of the refrigeration capacity is 'lost' through the cooling of the evaporator. In addition, the temperature of the compressor decreases during the off-cycle, which results in lower compressor efficiency when the compressor resumes operation. Cycling losses refer to the combination of these effects which have an adverse impact on the performance of the system.

Depending on the frequency at which the system cycles, these losses can reduce system performance by as much as 25% (Coulter and Bullard, 1997). However, they are not treated as a separate entity in his computer program since they are already embedded in the estimate of the cabinet load (refer to Section 4.3.1)

3.4 Inputs into the Program

The program requires input of the evaporator and condenser UAs, the effectiveness of the suction-line heat exchanger and the manufacturer's compressor maps, all of which are unique to each unit. While the program can accurately predict all outputs over a wide range of cabinet and ambient temperature combinations (refer to Section 3.4.4 for this range), the off-cycle time can only be predicted when the temperature of the freezer and refrigerator cabinets are set to 5°F and 38°F respectively, with the ambient fixed at 90°F. This is because the cabinet loads, which are used to calculate the off-cycle time (a detail discussion can be found in Section 3.5.2) are only available for this combination of temperatures.

3.4.1 Heat Exchanger UA

If fouling effects are negligible, the UA of the heat exchanger depends only on the heat transfer coefficient of the air and refrigerant, the conductivity of the tubes that carry the fluid and the available space for heat transfer, as shown in Eqn. 3.2 for an unfinned heat exchanger.

$$\frac{1}{UA_{HX}} = \frac{1}{h_{air} A_{ai} r} + \frac{\ln\left(\frac{r_{out}}{r_{in}}\right)}{2pkL} + \frac{1}{h_{refg} A_{refg}} \qquad \text{Eqn. 3.2}$$

Due to its lower heat transfer coefficient, the majority of the resistance to heat transfer is usually supplied by the air side. For this reason, it is unlikely that the change in the mass flow rate (which affects the heat transfer coefficient) of refrigerant should have a significant

effect on the conductance of the heat exchanger. This allows the UA for the evaporators and condenser to be expressed only as a function of the airflow rate based on the experimental measurements described in Chapter 4, as shown below.

$$UA = a_0 + a_1 CFM^{0.8} \qquad \text{Eqn. 3.3}$$

where a_0 and a_1 are empirically derived coefficients. Hence, the airflow rate through the evaporator and condenser must be specified to enable the UA of the heat exchanger to be calculated.

3.4.2 Effectiveness of the Suction-Line Heat Exchangers

In the previous chapter, measurements were performed to measure the UA of the heat exchangers and the effectiveness of the suction-line heat exchangers in the system. The results have shown that the effectiveness of the suction-line exchangers in both the freezer and the refrigerator exceed 90%. In addition, the pressure drop across the suction-line heat exchangers was estimated to be approximately 0.1 psi in Chapter 5. To be on the conservative side, the effectiveness of these devices was fixed at 0.9 while the pressure drop was set at 0.5 psi.

3.4.3 Cabinet Loads (Reverse Heat Leak Test vs. UA Experiments)

The cabinet cooling load, which is a measure of the load that the compressor has to satisfy, is a function of the ambient and cabinet setpoint temperatures. To determine the cabinet loads, a reverse heat leak test was performed by the manufacturer of this refrigerator. In this test, the temperature of the freezer and refrigerator cabinets was set to 90°F and 45°F respectively while the ambient was kept at 5°F. Owing to the reversal in operating conditions, heat must instead be supplied to the cabinet to maintain it at a higher temperature than the surroundings. Heat is provided by placing electrical heaters in the cabinet. The amount of energy that is supplied to the heaters is then a measure of the apparent loads that result from the difference between the cabinet and ambient temperatures.

While a reverse heat leak test can provide a good estimate of the actual cabinet load, it fails to account for cycling losses and the effect of any heat escaping back into cabinet from the mullion tubes. During normal operation, warm refrigerant from the compressor discharge is circulated around the cabinet to prevent the condensation of water vapor on its outer surface. As the reverse heat leak test is only concerned with the amount of energy that the heaters consume, no refrigerant is pumped around the cycle and the heat that normally escapes back into the cabinet is not measured. The amount of heat that these mullion tubes reject into the cabinet is discussed in further detail in Chapter 7.

Since heat is supplied to the cabinet by a set of electric heaters, cycling losses cannot be measured by this test. Even if the heaters were repeatedly turned on and off to mimic the cycling of a compressor, there will be no energy (cycling) loss associated with such an action. In addition to the failure of the heat leak test in measuring cycling losses and mullion heat rejection, the heat discharged by the evaporator fan has an opposite effect on the heat

leak test as it does during the actual operation of the refrigerator. In stead of contributing towards the cooling load of the cabinet, the heat released by the evaporator fan motor decreases the amount of energy that the heaters consume.

As an alternative to the estimates from the manufacturer's test, the UA experiments from Chapters 2 and 4 can be used to calculate the cooling load of the freezer and refrigerator cabinets (refer to Section 4.3.1 for the method of computation). There are two major differences between the reverse heat leak test and the UA experiments. The ability of the UA experiment to measure the effects of mullion heat rejection and cycling losses constitutes the first while the second involves the difference in the combination of the cabinet and ambient air temperatures between the two methods.

In the reverse heat leak test, the ambient was kept at 5°F while the freezer and refrigerator cabinet temperatures were set at 90°F and 45°F respectively. With this combination of temperatures, the difference between the cabinet and ambient temperature was 85°F for the freezer and 40°F for the refrigerator. On the other hand, the setpoint temperatures of the freezer and refrigerator cabinet were 5°F and 38°F, respectively, while the ambient was kept at 90°F in the UA experiments. Although the difference between the freezer and ambient temperatures remains the same, the difference between the refrigerator and ambient temperature was larger in the UA experiments. Due to this larger temperature difference, the estimate of the refrigerator load based on the UA experiments was undoubtedly higher. Aside from the difference between the freezer cabinet and ambient temperatures, the cabinet load for the freezer is also dictated by the temperature in the refrigerator cabinet due to the heat flow from the refrigerator to the freezer. Because of the

greater temperature difference between the refrigerator and the freezer in the reverse heat leak test, this method produces a larger estimate of the freezer cooling load.

Owing to the differences between the reverse heat leak test and the UA experiments, the estimate of the cabinet load was different for both methods. While cycling losses and mullion heat rejection increases the estimated loads of both cabinets, the combination of cabinet and ambient temperatures in the UA experiment tends to underestimate the freezer cabinet load and overestimate the refrigerator cabinet load.

As a result of these combined effects, the freezer cabinet load obtained from the UA experiments (276 Btu/hr) was 16% higher than the reverse heat leak test (232 Btu/hr). A comparison is only possible for one airflow rate, that is for an airflow of 57 CFM in the freezer evaporator because the heat leak test was only performed for this airflow. For the refrigerator, the estimated load from the UA experiments (197 Btu/hr) was 33% larger than the estimate from the heat leak test (132 Btu/hr). The comparison here is for the case of 25 CFM airflow across the refrigerator evaporator.

There are two advantages of using the results that were obtained from the UA experiments. Apart from its ability to replicate the actual conditions that the freezer and refrigerator operate under (by accounting for cycling losses and heat leaking into the cabinet), another advantage is the fact that the UA experiment was also conducted over a range of airflow rates. Therefore, the change in the cabinet load as a function of the airflow (or evaporator UA) was also explored by this method (discussed in Section 4.3.1). In contrast, the reverse heat leak test was only performed for a single evaporator fan speed, and the load was assumed to be independent of the airflow rate. In view of the advantages of using the values from the UA experiment, both the freezer and refrigerator cooling loads

were expressed in terms the evaporator UA (a linear fit had provided sufficient accuracy, Figures 4.5 and 4.6).

3.4.4 Manufacturer's Compressor Maps

Compressor maps are provided by compressor manufacturers to describe the performance of their product at different operating conditions. The information in these maps typically show the refrigeration capacity, compressor power and current draw as a function of different evaporating and condensing temperatures. The freezer compressor maps are only valid for evaporating temperatures between –30°F and 30°F and condensing temperatures between 100°F and 130°F. The range of these maps for the refrigerator compressor are from –30°F to 20°F and 100°F and 130°F.

3.4.4.1 Refrigeration Capacity

Using the maps supplied by the compressor manufacturers, the capacity was curve-fitted to the evaporating and condensing temperatures in the form of Eqn. 3.4.

$$Capacity_{map} = b_0 + b_1 T_{evap} + b_2 T_{evap}^2 + b_3 T_{evap}^3 + b_4 T_{con} + b_5 T_{con}^2 + b_6 T_{con}^3 + b_7 T_{evap} T_{con} + b_8 T_{evap}^2 T_{con} + b_9 T_{evap} T_{con}^2 + b_{10} T_{evap}^2 T_{con}^2 \quad \text{Eqn. 3.4}$$

where b_0, $b_1 \ldots b_{10}$ were all coefficients that provided the best fit. By fitting the curves to the cubic power with cross terms, the above equation was able to match the capacity curves from

the compressor maps to more than 99% accuracy (i.e. maximum deviation from the map was < 1%) with an R^2 value of 100%.

In producing the compressor maps, the manufacturers define the capacity of the compressor as the heat that is required to first evaporate the liquid refrigerant at 90°F that has been expanded across the capillary tube and subsequently superheated to 90°F at the saturated evaporating pressure. In other words, the capacity from the map was expressed as follows.

$$Capacity_{map} = \dot{m}_{map}\left(h_{90,evap} - h_{90,cond}\right) \qquad \text{Eqn. 3.5}$$

where $\dot{m}_{map}$ = mass flow rate of refrigerant according to the map
$h_{90,evap}$ = enthalpy of the refrigerant at 90°F at the evaporating pressure
$h_{90,cond}$ = enthalpy of the refrigerant at 90°F at the condensing pressure

Eqn. 3.5 is useful because it enables the mass flow rate of the refrigerant to be calculated. In most cases, however, the vapor that enters the compressor is at a temperature other than 90°F. With the density of the vapor being a function of temperature, the amount of mass that the compressor delivers will vary according to the suction conditions. As the rate of refrigerant mass flow directly influences the refrigeration effect, it should be corrected to reflect the conditions at the compressor inlet, as Eqn 3.6 shows.

$$\dot{m}_{actual} = \dot{m}_{map}\left(\frac{r_{evap,actual}}{r_{evap,90}}\right) \qquad \text{Eqn. 3.6}$$

where $\dot{m}_{actual}$ = actual mass flow rate of the cycle
$r_{evap,actual}$ = vapor density at the suction temperature and evaporating pressure
$r_{evap,90}$ = vapor density at 90°F at the evaporating pressure

The actual capacity that the compressor delivers may then be appropriately obtained by multiplying the actual mass flow rate with the difference in enthalpy of the refrigerant across the evaporator as follows.

$$Capacity_{actual} = \dot{m}_{actual}\left(h_{evap,out} - h_{evap,in}\right) \qquad \text{Eqn. 3.7}$$

In the previous chapter, experiments that were carried out to measure the UA of the coils in the freezer and refrigerator cycles were described. Aside from the temperature, pressure and airflow measurements, the compressor power consumption and mass flow rate of refrigerant were also recorded as a function of time during the on-cycle. By using the measured evaporating and condensing pressures (or temperatures), Eqn. 3.4 was used to determine the capacity and hence, the mass flow rate of the cycle. A comparison between the mass flow for the freezer cycle evaluated from the map and from actual mass flow measurements (using the mass flow meter) are plotted against time for a typical cycle in Figure 3.2.

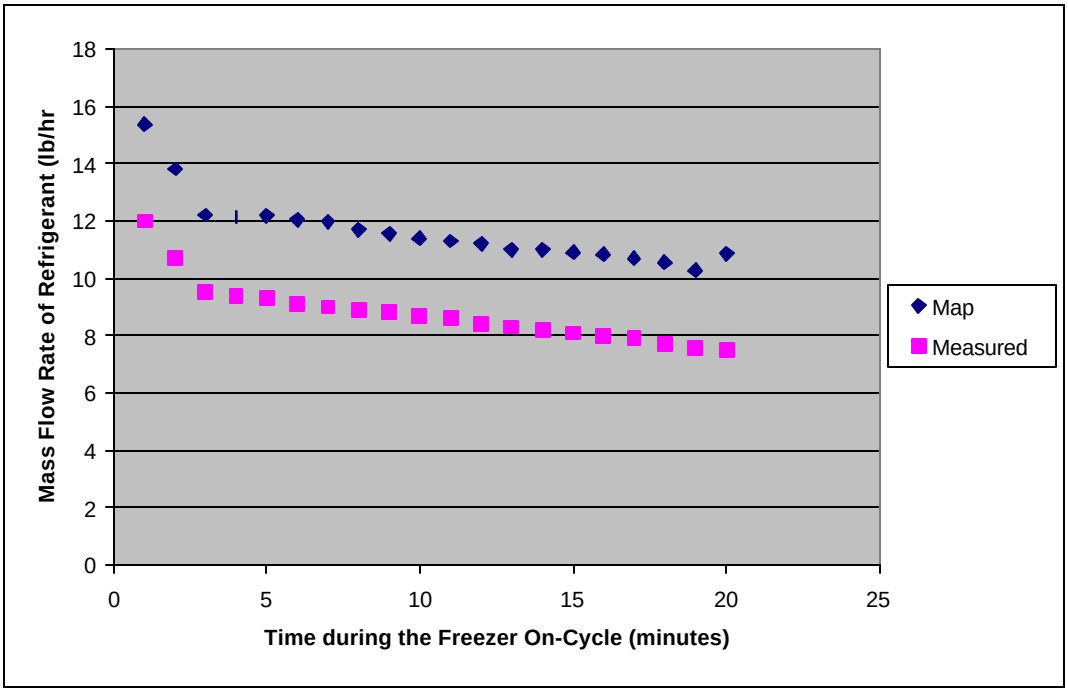

Figure 3.2 Predicted and actual mass flow in the freezer cycle as a function of time. The evaporator airflow was 57 CFM for this case.

It is clear that the compressor map consistently overpredicts the mass flow compared to the measured value. When using the maps, the mass flow rate was approximately 33% higher than that measured by the mass flow meter. While Figure 3.2 only illustrates the difference between the map predictions and measurements for one freezer evaporator airflow (57 CFM), Figure 3.3 shows this difference at other airflow rates.

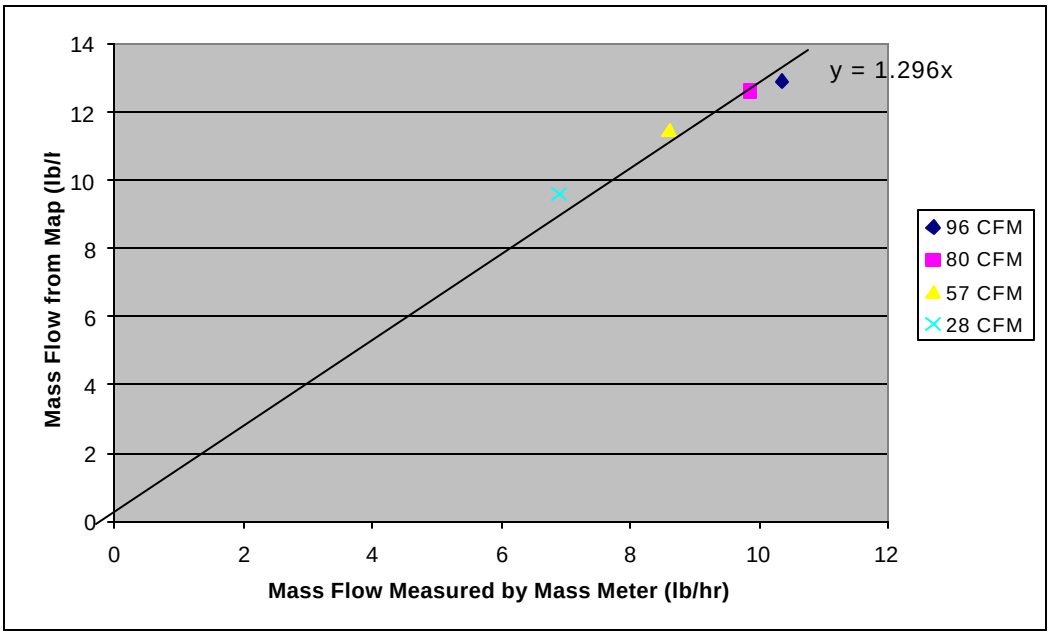

Figure 3.3 Comparison between the predicted and measured mass flow rate for different freezer evaporator airflow rates.

In the above plot, the single point for each airflow represents the averaged mass flow over an entire cycle (many such cycles were analyzed and the points in Figure 3.3 show their average). Since the refrigeration capacity is directly proportional to its mass flow, it is essential to account for this discrepancy. To ensure that the maps were able to make accurate predictions, the curve-fit equation for the capacity in the form of Eqn. 3.4 was modified by dividing it by an empirically derived factor. In other words, this constant represents a proportionality factor that is used to reconcile the unexplained differences between the measurements and the map predictions. The value of this constant, which represents the ratio of the map predictions to the measured mass flow, was obtained from Figure 3.3 as 1.3.

A similar correction was also required for the refrigerator compressor maps. Figures 3.4 and 3.5 are similar to Figures 3.2 and 3.3 respectively, but they represent typical refrigerator cycles.

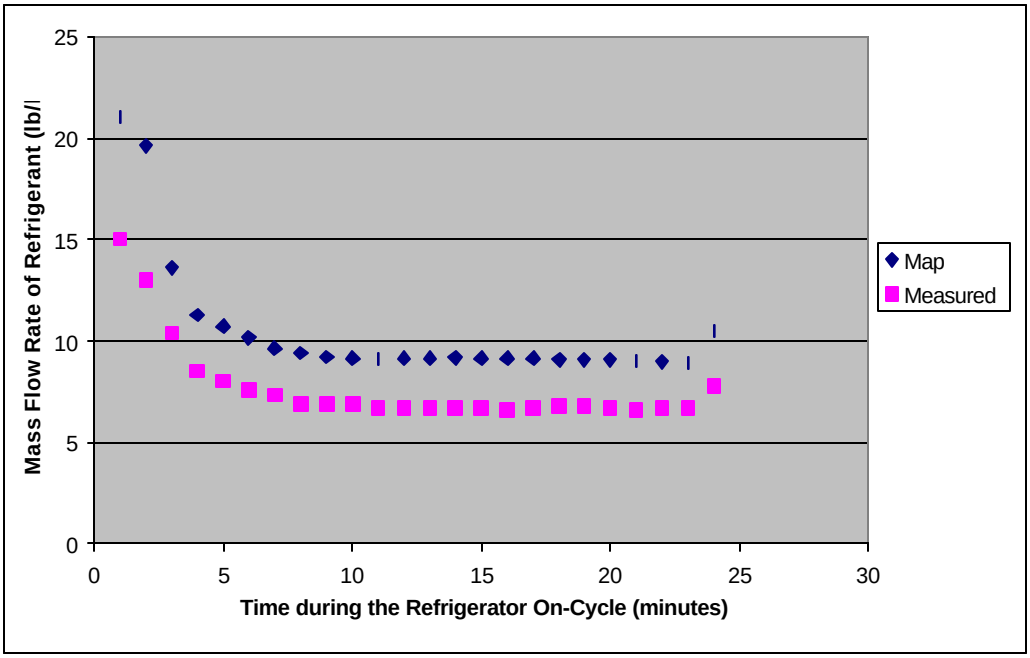

Figure 3.4 Predicted and actual mass flow in the refrigerator cycle as a function of time. The evaporator airflow was 25 CFM for this case.

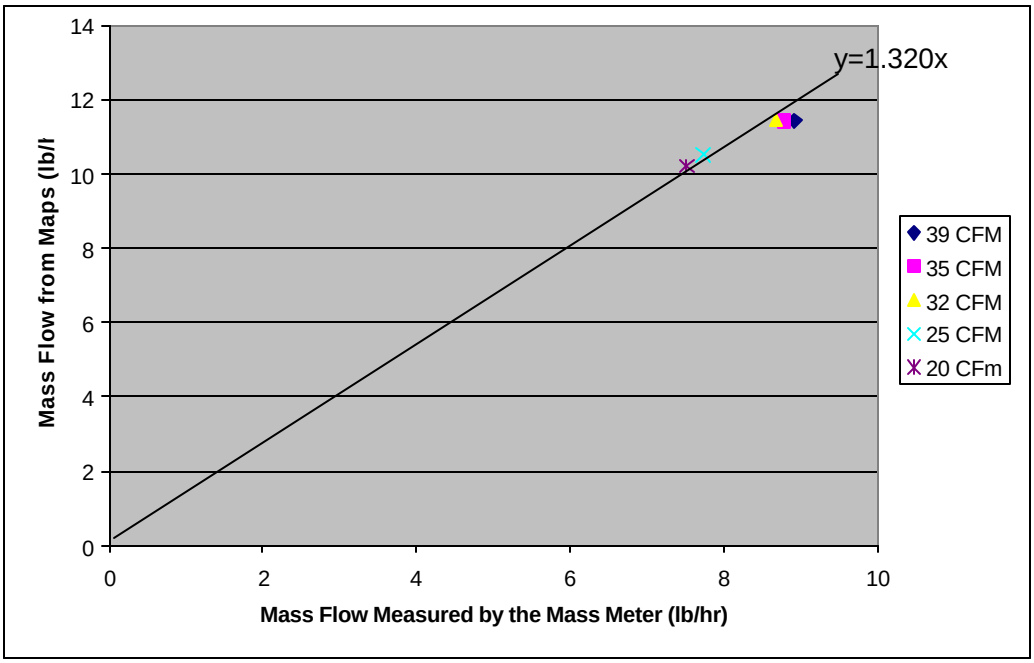

Figure 3.5 Comparison between the measured and predicted mass flow rate for different refrigerator evaporator airflow rates.

The above plot shows that the predictions from the map were about 32% higher than those measured. In addition, the airflow rate was seen to have little impact on this overestimation (i.e. the percentage of the overestimate was consistently around 32% over all the airflow rates studied). The appropriate value of the constant which must be used to modify Eqn. 3.4 for the refrigerator compressor is then 1.32.

3.4.4.2 Compressor Power Consumption

As with the capacity, the compressor power is a function of the evaporating and condensing temperatures. This relationship is modeled using the form shown in Eqn. 3.8.

$$Power_{map} = c_0 + c_1 T_{evap} + c_2 T_{evap}^2 + c_3 T_{con} + c_4 T_{con}^2 + c_5 T_{evap} T_{con} \qquad \text{Eqn. 3.8}$$

where c_0, c_1, $\ldots c_5$ are curve-fitting coefficients. For the curve fit to the compressor power, a quadratic with cross terms was sufficient to yield predictions that had a maximum deviation from the compressor map of less than 2%. The R^2 value for this fit was 99.8%.

While a change in the specific volume of the suction gas affects the capacity of refrigeration, it has no impact on the power drawn by the compressor (this fact is discussed in detail in Section 5.2).

For a fixed compressor and refrigerant, the power is only a function of the evaporating and condensing temperatures. With the power being independent of the suction vapor temperature, the calculated refrigerant mass flow rate from the map may be used to determine the change in the enthalpy of the refrigerant across the compressor, as shown in Eqn. 3.9.

$$Power_{map} = \dot{m}_{map}\left(h_{comp,out} - h_{comp,in}\right) \qquad \text{Eqn. 3.9}$$

Just as the curve-fitted equation for the refrigeration capacity needs to be modified to account for the differences between the map estimates and the actual measurements, the power was also subjected to the same problem. A similar trend was observed here, whereby the measured power was also consistently lower than the predicted power from the maps. Figure 3.6 shows this difference for one airflow rate through the freezer evaporator while Figure 3.7 shows the average power consumption over one cycle for five different airflow rates.

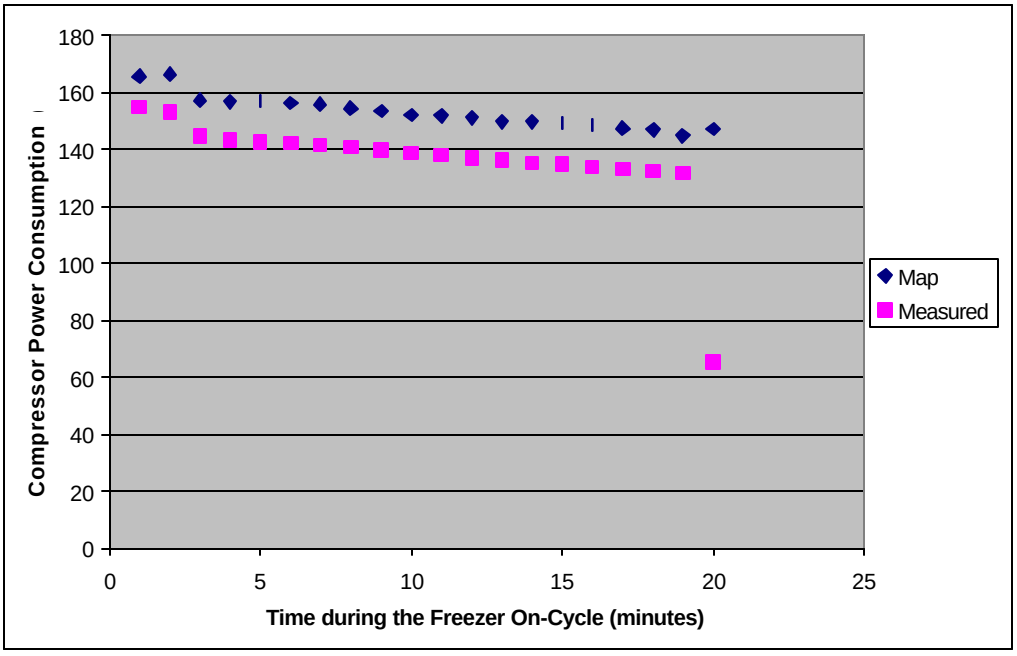

Figure 3.6 Predicted and actual power drawn by the freezer compressor as a function of time. The evaporator airflow was 57 CFM for this case.

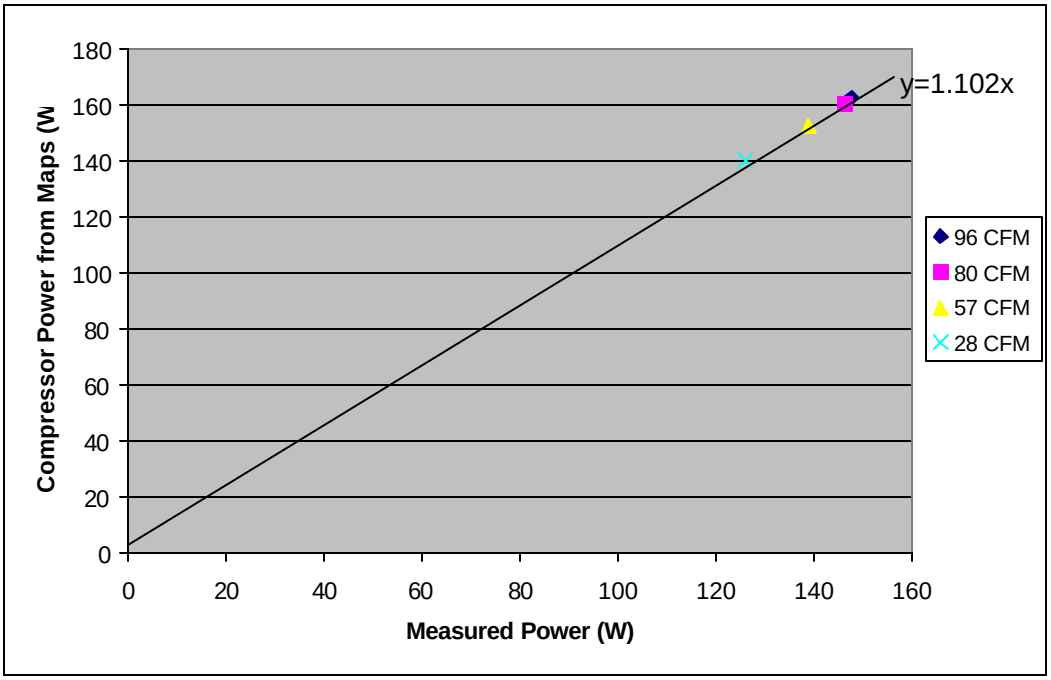

Figure 3.7 Comparison between the measured and predicted power for different freezer evaporator airflow rates.

Figure 3.7 shows that the power predicted from the maps was 10% above the actual power that was drawn by the freezer compressor. The change in airflow rate was also seen to have a negligible effect on this difference. Therefore, the compressor map for the freezer compressor power will have to be divided by 1.1 to yield accurate predictions. To determine the deviations of the maps from the actual measurements for the refrigerator compressor, Figures 3.8 and 3.9 show the same plots as Figures 3.6 and 3.7, but for the refrigerator cycle.

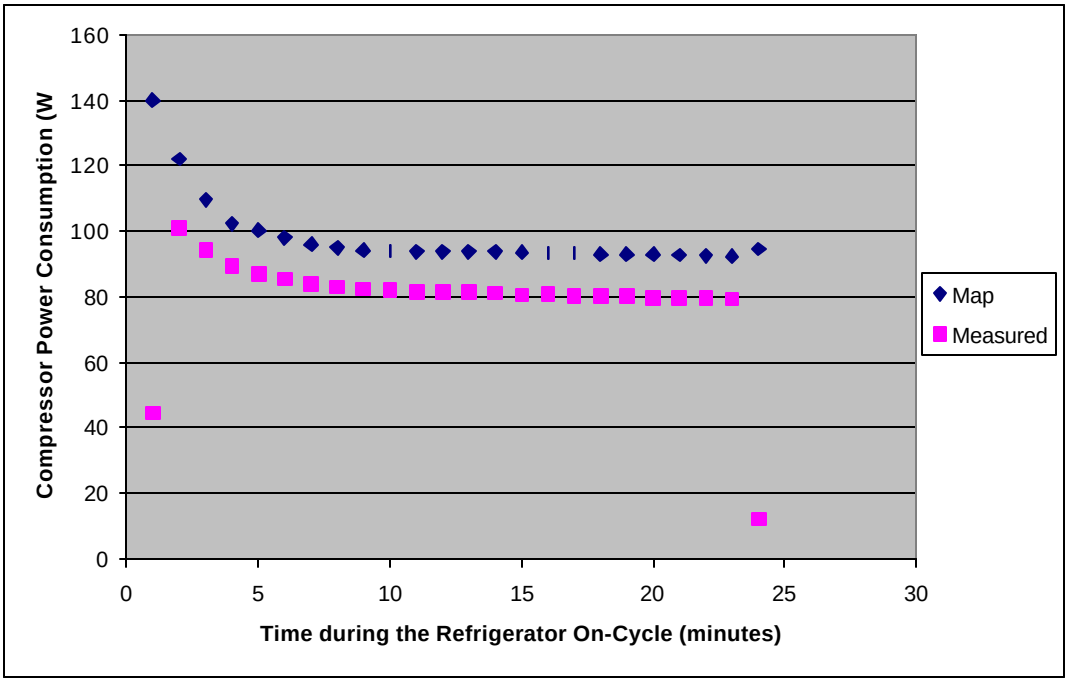

Figure 3.8 Predicted and actual power drawn by the refrigerator compressor as a function of time. The evaporator airflow was 25 CFM for this case.

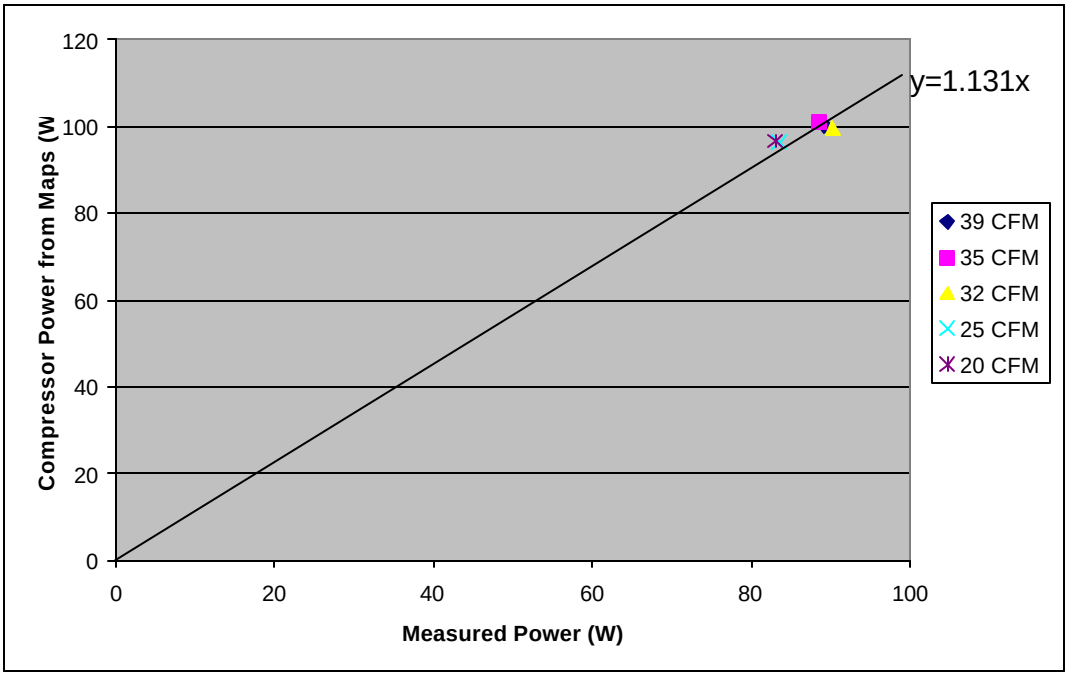

Figure 3.9 Comparison between the measured and predicted power for different refrigerator evaporator airflow rates.

For the refrigerator, the map estimates were higher by an average of 13% over the five airflow rates studied. The empirically derived factors that need to be applied to the curve-fit equations of the capacity and power are summarized in Table 3.1 for the refrigerator and freezer.

	Refrigeration Capacity	**Compressor Power**
Freezer	1.30	1.10
Refrigerator	1.32	1.13

Table 3.1 The factors that were used to modify the curve-fit equations.

The factors in Table 3.1 show that the freezer maps were slightly more accurate than the refrigerator. For both compressors, the error in the capacity predictions was much larger than the power. This suggests that the maps tend to overestimate the COP of the cycles by as much as 18% for the freezer and 17% for the refrigerator.

3.5 Output of the Programs

3.5.1 Refrigeration Capacity and Compressor Power Consumption

The refrigeration capacity and compressor power consumption are the most important outputs in this program as they provide a measure of the impact of the proposals that will be studied. By performing an energy balance on all the components and using the inputs and assumptions described above, all the equations are all solved simultaneously to yield the

evaporating and condensing temperatures and hence, the capacity (Eqn. 3.7) and power consumed by the compressor (Eqn. 3.9).

3.5.2 On and Off-Cycle Times

Aside from the refrigeration capacity and compressor power consumption, the on and off-cycle times are of interest as they determine the number of cycles that the compressor executes in a day. In Chapter 4, the UAs of the freezer and refrigerator evaporators were experimentally measured for different airflow rates. Similarly, the on and off-cycle times that accompany the change in UA were also recorded. A larger UA enhances the heat transfer process and increases the capacity for refrigeration, so the cycle run times are reduced. At the same time, the off-cycle times are shorter when an evaporator with a larger UA is installed. Although the exact explanation for this observation is still uncertain, it is most likely due to the effects of air stratification in the cabinets (a further discussion on this topic is covered in Section 4.3.1).

Based on the inputs and the energy balances alone, this program is not capable of predicting both the on and off-cycle times. The percentage of time that the compressor operates may be determined by dividing the cabinet load by the refrigeration capacity. But the percentage alone only gives the ratio of the on-cycle time to that of the sum of the on and off cycles times together (total time for one complete cycle), as Eqn. 3.10 shows.

$$\frac{CabinetLoad}{Capacity} = \frac{OnCycleTime}{OnCycleTime + OffCycleTime} \qquad \text{Eqn. 3.10}$$

To obtain the value of both parameters, either the on or off-cycle times or an expression that relates these two parameters must be independently supplied. Since the nature of the on-cycle time response to the change in evaporator UA was better understood, the on-cycle time was expressed as a function of the evaporator UA in this program, as shown in Eqn. 3.11.

$$OnCycleTime = d_0 + d_1 UA_{evap} + d_2 UA_{evap}^2 + d_3 UA_{evap}^3 \qquad \text{Eqn. 3.11}$$

where d_0, d_1, d_2 and d_3 are all coefficients. Although the evaporator UA in Eqn 3.11 is assumed to be independent of time (by taking its average over the on-cycle), is depends on the airflow rate. With a given airflow rate, the evaporator UA may be determined using Eqn 3.3 and subsequently used in Eqn. 3.11 to yield on-cycle time. Finally, the off-cycle time is calculated from Eqn. 3.10 when the on-cycle time is known.

3.6 How the Program Works

Having explained the assumptions, inputs and the outputs, the following figure summarizes their role in the computer program.

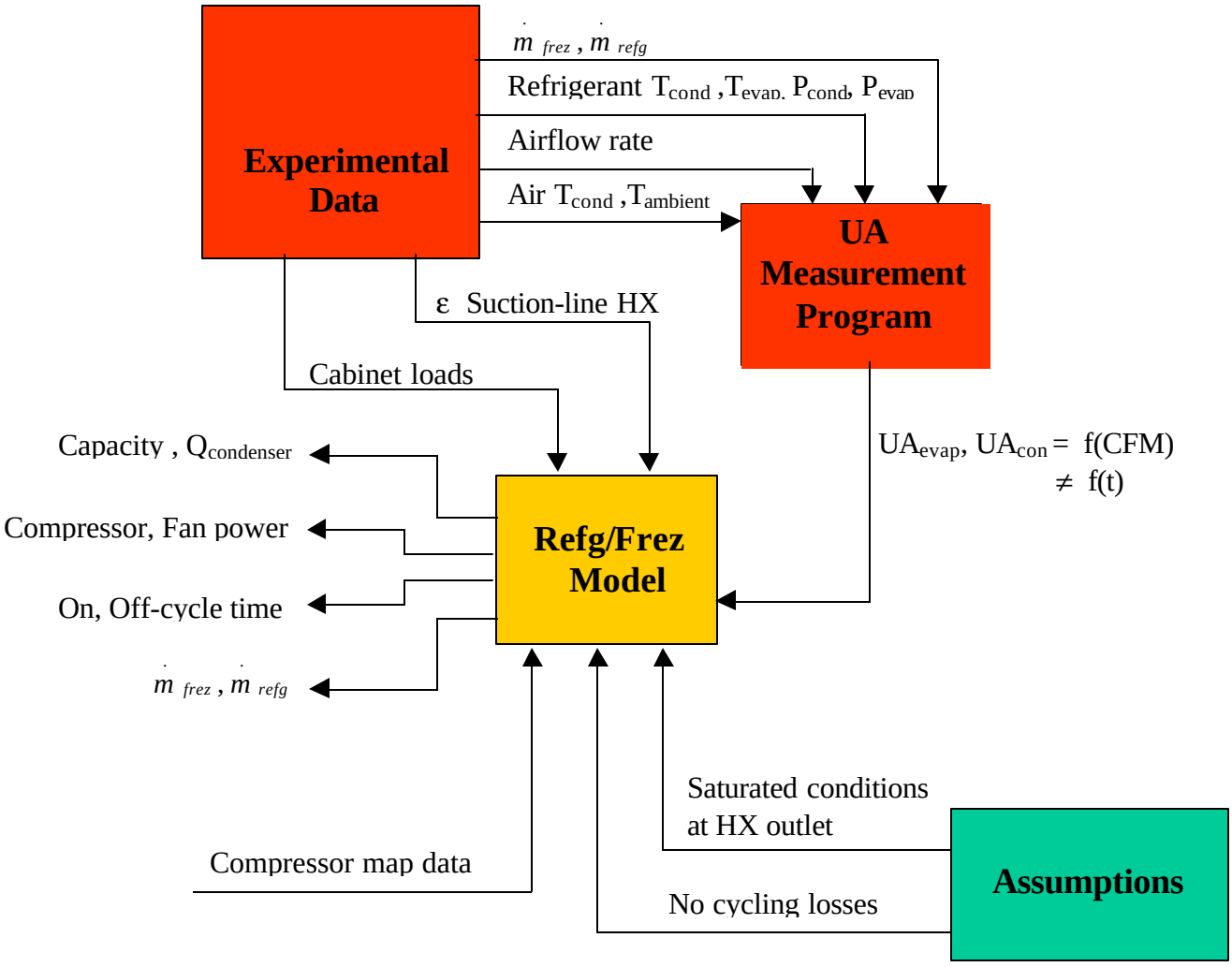

Figure 3.10 Overall picture of how the program works.

3.7 Comparison between Model Outputs and Actual Measurements

To demonstrate that the program is capable of simulating the performance of the refrigerator, the outputs from the calculations should match the measured values as closely as possible. The most important outputs are the refrigeration capacity, compressor power consumption and the amount of time that the compressor spends in the on and off-cycle mode. While the compressor energy consumption and the on and off-cycle times were experimentally measured, the capacity of refrigeration could not be obtained form the experiment. Although the capacity predicted by the model cannot be experimentally verified, the accuracy of this prediction can be determined by comparing the off-cycle time from the experiment and the program. This is because the capacity is required to calculate the off-cycle time in Eqn. 3.10.

The measured and predicted total energy consumption of the compressor and fans (evaporator and condenser) per cycle for the freezer is tabulated below.

Condenser airflow rate (CFM)	**Evaporator airflow rate (CFM)**	**Measured energy/cycle (Wh)**		**Predicted energy/cycle (Wh)**
		Set 1	**Set 2**	
124	28	66.9 - 68.3	65.6 - 67.0	65.3
124	57	51.7 - 52.7	52.3 - 53.3	51.7
124	80	43.8 - 44.7	43.8 - 44.9	46.3
124	96	45.1 - 46.1	45.4 - 46.7	46.6

Table 3.2 Comparison between the measured and predicted energy per cycle for the freezer.

The figures for the measured energy/cycle in Table 3.2 represent the range of values observed during the test (only freezer cycles that did not coincide with the refrigerator cycle were considered). Table 3.2 shows two sets of data that were taken over two separate weeks.

The model was calibrated (i.e. data that was used to determine the heat exchanger UAs and the constants in Table 3.1) using data obtained from Set 1. The second set of data was included to show that the results from the program were also in good agreement with data that was not used in its calibration. A comparison between the data from Set 1 and Set 2 also confirms that the tests are repeatable. The results show that at lower airflow rates, the predictions were smaller than the experimental measurements while the converse was true at higher airflow rates. In all, the results show that most of the predictions were very close or had fallen within the range of values measured.

Table 3.3 shows the comparison between the actual and predicted off-cycle times for the freezer (the on-cycle time in the program was curve-fitted to that measured and should therefore be the same, so they are not included in this table).

Condenser airflow rate (CFM)	**Evaporator airflow rate (CFM)**	**Measured off-cycle time (minutes)**		**Predicted off-cycle time (minutes)**
		Set 1	**Set 2**	
124	28	32 - 33	32 - 33	32.9
124	57	29 - 30	29 - 30	30.2
124	80	26 - 27	26 - 28	27.1
124	96	26 - 27	26 - 27	27.2

Table 3.3 Comparison between the measured and predicted off cycle-time for the freezer.

The off-cycle times for both sets of experimental data again confirm that the experiments were repeatable. The accurate prediction of the refrigeration capacity has enabled the off-cycle time from the program to compare very favorably to that measured.

The same analysis was made for the parameters that were associated with the refrigerator. Tables 3.4 and 3.5 show that the comparison for the refrigerator parameters was

just as good as the freezer. However, the experimental data exhibits a higher degree of scatter, particularly in the off-cycle time. Unlike the freezer, the off-cycle time for the refrigerator is less consistent form one set of tests to another. The differences, though, is only very small and is not of great concern.

Condenser airflow rate (CFM)	Evaporator airflow rate (CFM)	Measured energy/cycle (Wh)		Predicted energy/cycle (Wh)
		Set 1	Set 2	
124	20	45.8 - 47.8	45.5 - 47.7	47.0
124	25	44.1 - 45.5	43.0 - 44.8	44.3
124	32	51.9 - 53.9	50.8 - 52.6	50.1
124	35	54.4 - 55.8	53.9 - 55.5	53.3
124	39	56.7 - 58.0	55.8 - 57.0	57.1

Table 3.4 Comparison between the measured and predicted energy per cycle for the refrigerator.

Condenser airflow rate (CFM)	Evaporator airflow rate (CFM)	Measured off-cycle time (minutes)		Predicted off-cycle time (minutes)
		Set 1	Set 2	
124	20	52 - 54	51 - 54	51.9
124	25	48 - 50	48 - 51	49.1
124	32	52 - 55	52 - 54	52.8
124	35	55 - 57	54 - 56	55.2
124	39	55 - 58	55 - 56	56.9

Table 3.5 Comparison between the measured and predicted off cycle-time for the refrigerator.

3.8 Conclusions

A computer program, which employs a quasi steady-state model, was developed to simulate the performance of the refrigerator. Together with some inputs and assumptions, the program functions by performing energy balances on every component in the vapor-compression cycle. Specifically, the program calls for the input of the heat exchanger UAs, suction-line heat exchanger effectiveness, cabinet loads and compressor maps. In order to solve for the outputs, the assumption of saturated conditions at the outlet of the evaporators and condenser and negligible losses due to the cycling of the compressor were made. Among others, the program is capable of predicting the refrigeration capacity, compressor power consumption and the on-cycle times over a wide range of operating temperatures. However, an accurate prediction of the off-cycle time is only possible when the freezer and refrigerator cabinet temperatures are set at 5°F and 38°F respectively with the ambient kept at 90°F because the cooling loads (determined from the UA experiments) are only available for this combination of temperatures.

While the compressor maps were supplied by the manufacturer, they had to be corrected based on the vapor temperature at the suction line as it may differ from the conditions at which the compressor was rated. In addition to this correction, experimental data have shown that both the freezer and refrigerator compressor maps had overestimated the capacity by about 30% and the power by as much as 13%. To overcome this problem, the curve-fitted equations that expressed the capacity of refrigeration and compressor power as a function of the evaporating and condensing temperatures were modified by dividing it with an appropriate constant. These constants, which are a measure of the error in the

compressor maps, were obtained by comparing the experimental measurements to the map predictions.

The results show that the predictions made by the computer program compare favorably with experimental measurements. The fact that the program employs a quasi steady-state model in the analysis represents the largest source of error in the predictions. By using a quasi steady-state approach to model a transient process, the outputs in the program (particularly the refrigeration capacity) loses the ability to respond to any changes in the system, like the evaporating temperature, with time. In any case, the differences between the measurements and the computer predictions are small, which is essential if it were to be used as a tool to evaluate the proposals to be studied in the coming chapters.

CHAPTER 4 Sizing of Heat Exchangers

4.1 Introduction

The sizing of heat exchangers remains essential in ensuring that the system operates at its optimum. Heat exchanger sizing involves the physical sizing of this component and the fan that influences the heat transfer coefficient of the process. A properly designed heat exchanger can enhance system performance. If the current heat exchanger is undersized, system performance will suffer. On the other hand, a higher system cost may be difficult to justify if the heat exchanger is oversized. For this purpose, experiments were carried out to determine the conductance value of the current heat exchangers, and the effect of different airflow rates on the UA of the coils and the performance of the system.

4.2 Experimental Setup and Procedure

One of the objectives of this study was to investigate the savings that DC fans demonstrate when compared to their conventional AC counterparts. Besides the potential energy savings of using these fans, the lower energy consumption would also reduce the portion of cabinet load that results from the conversion of electrical energy to heat by these fan motors. While DC fans were used in both the refrigerator and freezer evaporators, only the existing AC fan was available for testing in the condenser.

The setup of the experiment was identical to that described in Section 2.2. After setting the speed on the three heat exchanger (freezer and refrigerator evaporators and condenser) fans, the unit was allowed to operate and data were collected over a 20-hour period. This procedure was repeated by varying the speed for only one fan while maintaining the fan speed for the other two heat exchanger fans. A similar procedure was carried out for the fans in the other two coils, one at a time.

4.3 Analysis of Results and Discussion

The measurements performed here were an extension of the procedure described in Chapter 2. Instead of calculating the UA for a particular airflow, measurements were performed over a wide range of fan speeds. Because of the identical set of conditions and equipment used for this experiment, the sources of uncertainty were the same. Specifically, errors in temperature and airflow measurements, together with the assumption of 100% sensible cooling at the evaporator, were the major contributors to the experimental uncertainties.

The change in UA as a function of airflow for all three heat exchangers is shown in Figures 4.1-4.4. The UA measurements represent an average taken over many cycles during the test. Error bars, which were calculated from a propagation of error analysis, have been included to indicate the amount of uncertainties associated with each measurement.

The operations of the refrigerator and freezer cycles are controlled independently. Since the UA of a heat exchanger is related to the available area for heat transfer and both cycles depend on the condenser as the source of heat rejection, the simultaneous running of both cycles will significantly influence the measurement of the condenser UA. To avoid the effects of simultaneous runs from interfering with the impact of a larger airflow on the heat condenser UA, only freezer and refrigerator cycles that run separately were considered in the analysis in Figures 4.1-4.4.

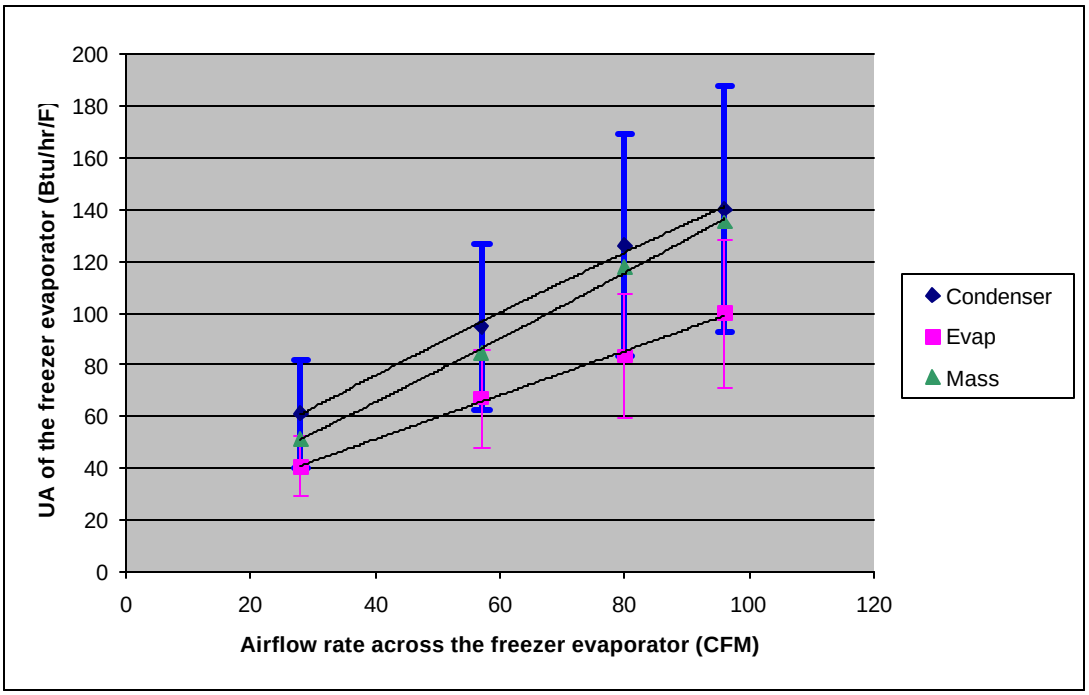

Figure 4.1 The change in freezer evaporator UA with airflow rate.

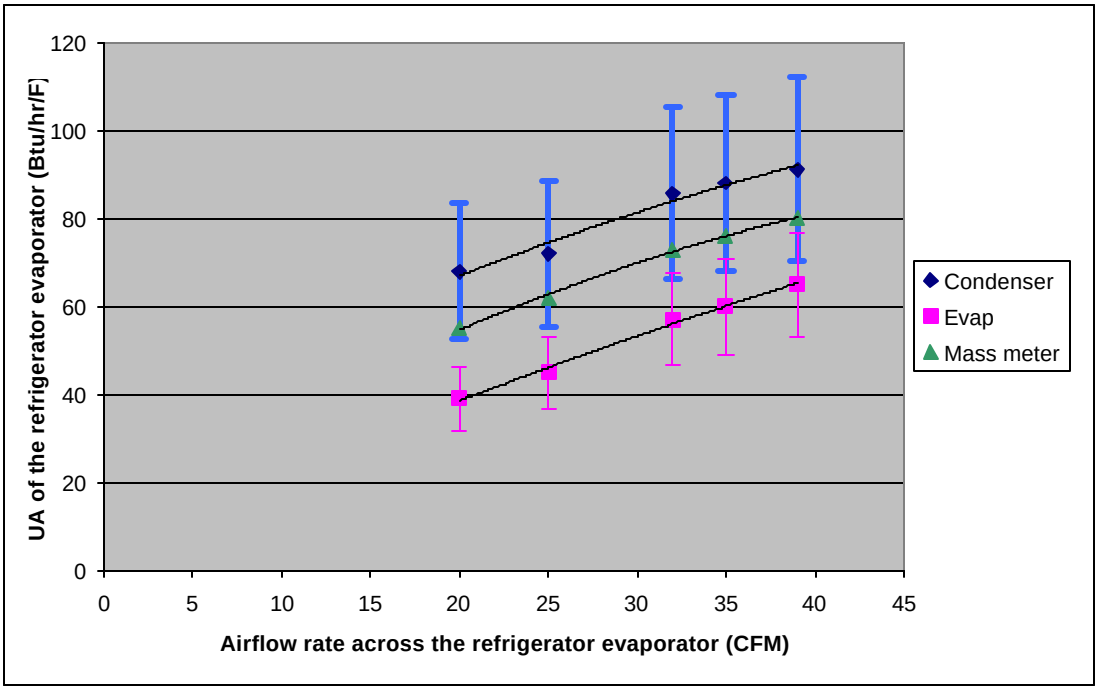

Figure 4.2 The change in refrigerator evaporator UA with airflow rate.

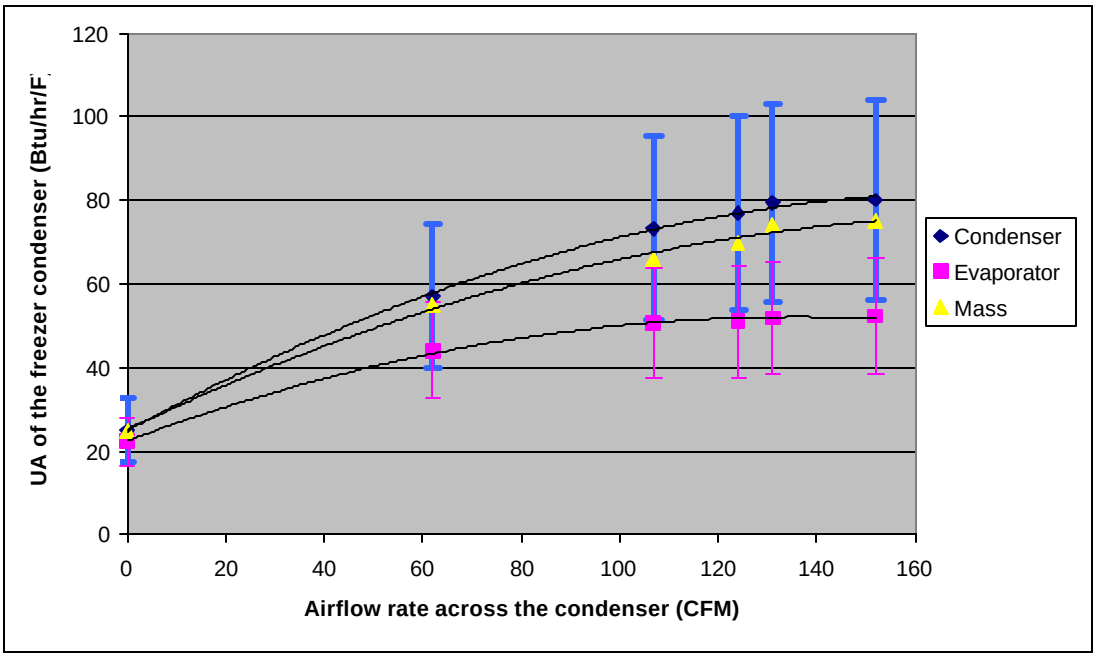

Figure 4.3 The change in condenser UA with airflow rate during the freezer on-cycle.

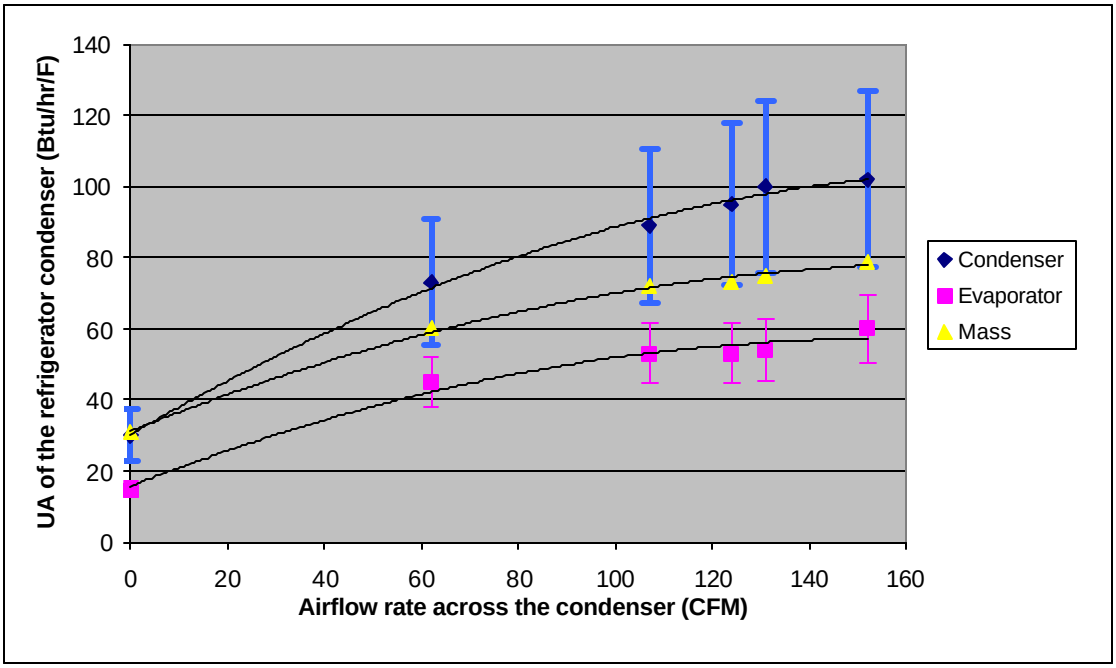

Figure 4.4 The change in condenser UA with airflow rate during the refrigerator on-cycle.

There are a few things to note from the UA vs. CFM curves. Firstly, the trends observed from the measurements in Chapter 2 are still preserved here. Calculations based on the condenser had remained the highest estimates, followed by the mass flow meter and then the evaporator. While the error bars had confirmed that the condenser measurements were within the boundaries of experimental uncertainty, the results obtained by performing an energy balance on the evaporator were not as reliable. The explanations offered in Chapter 2 to account for this observation equally apply here.

Secondly, the condenser UA was slightly different (5-10% higher for the refrigerator) between the two cycles, even though they share the same condenser. This result can be explained by the different tube arrangement and heat transfer surface that is dedicated to each cycle in the condenser. Because of a larger condenser load, the refrigerator cycle has an extra row of tubes to promote the rejection of heat to the environment. In addition, air

entering the condenser encounters the two rows of refrigerator tubes first before reaching the freezer tubes (this has no effect on the analysis if only cycles that run separately were considered).

Thirdly, the UA does not approach zero when the condenser fan was turned off. In the absence of the fan as a forcing agent, natural convection plays an important role in the heat transfer process. Since the airflow associated with natural convection is not easily calculated (not even possible here without the surface temperature of the condenser), the UA could not be calculated with an energy balance on the condenser. The UA could, however, be measured by performing an energy balance on the evaporator or using the mass flow meter measurements.

4.3.1 Cabinet Load as a Function of CFM

The possible enhancement in system performance remains the main goal of increasing the size of a heat exchanger. As much as an evaporator with a large UA may increase its ability to perform cooling, it is clear that the increase in performance should, at least, be adequate in offsetting the probable increase in cabinet load at higher airflow rates.

Using the data collected from the experiment, the average cabinet load per hour was calculated using Eqn. 4.1 and plotted as a function of airflow rate in Figures 4.5 and 4.6 for the freezer and refrigerator cycles respectively.

$$CabinetLoad = \frac{\int_{0}^{24hours} \dot{m}\left(h_{evap,out} - h_{evap,in}\right)}{24} \qquad \text{Eqn. 4.1}$$

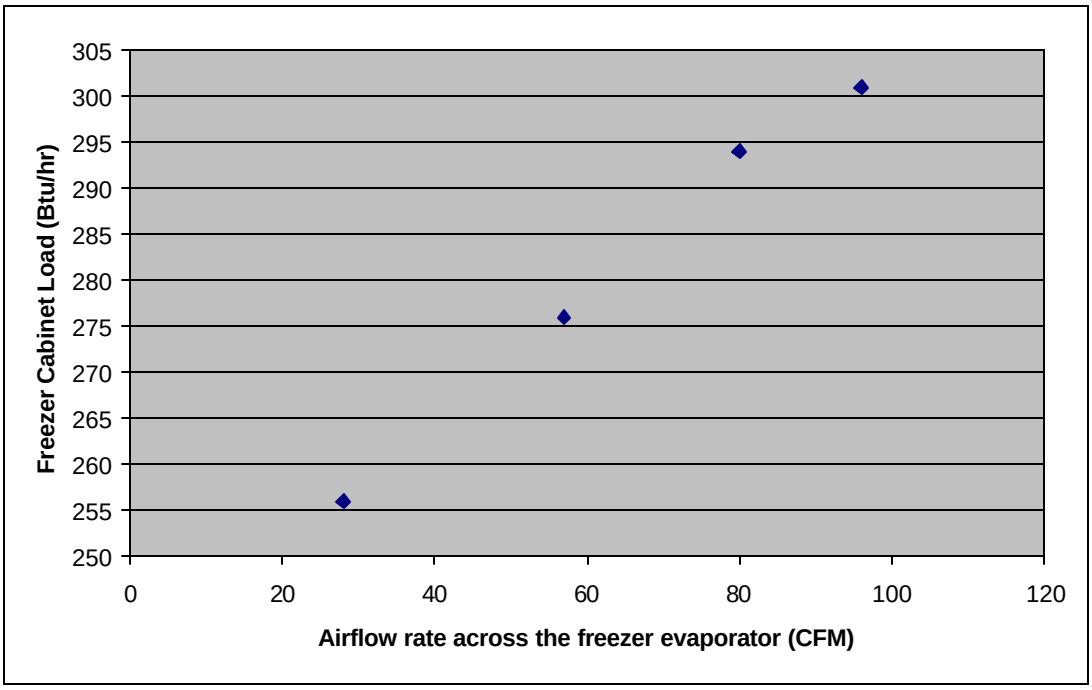

Figure 4.5 The freezer cabinet load as a function of the airflow rate.

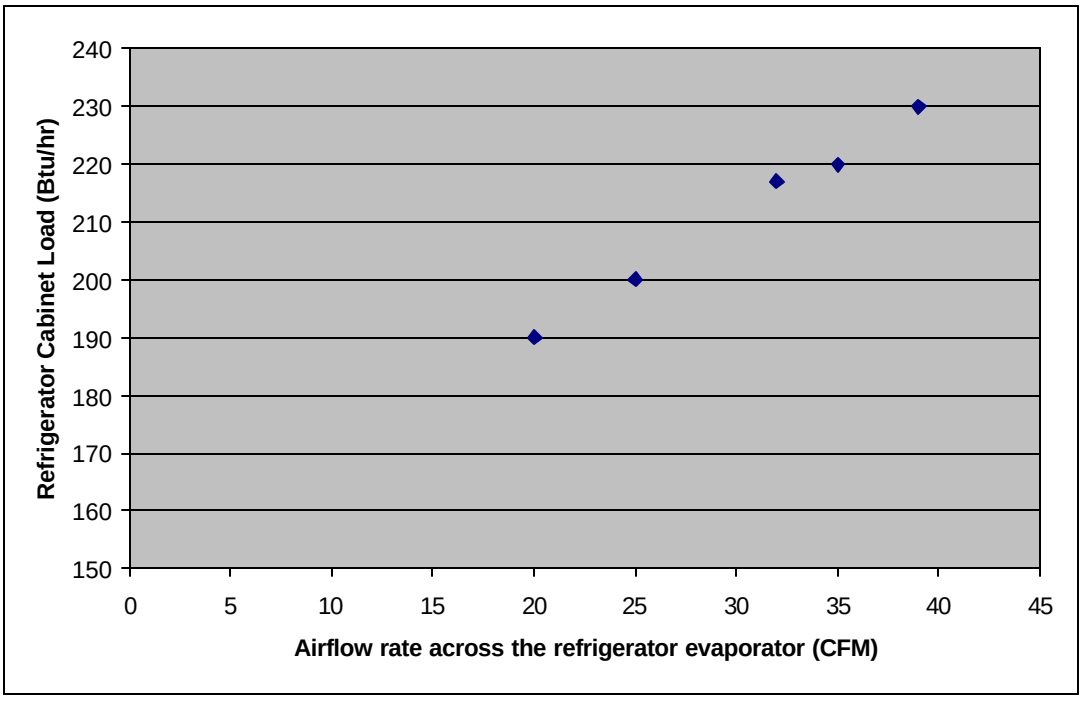

Figure 4.6 The refrigerator cabinet load as a function of the airflow rate.

For the sake of comparison, the load on the freezer cabinet, based on a reverse heat leak test performed by the refrigerator manufacturer, was 232 Btu/hr, while that obtained by way of Eqn. 4.1 was 276 Btu/hr. A similar test was performed by the manufacturer to measure the refrigerator cabinet load, but a comparison is not appropriate as the test was performed with a different combination of cabinet and ambient temperatures. The discrepancy between these figures is mainly due to the inability of the heat leak test to account for cycling losses and the heat escaping back into the cabinet from the mullion tubes that circulate the frame (refer to Section 3.4.3 for a detailed explanation).

Clearly, the load varies according to the rate of airflow in an almost linear fashion. A number of reasons that may possibly explain the response of the cabinet load to a change in the airflow rate will be examined here. Figures 4.7 and 4.8 show the temperature of the freezer and refrigerator cabinets over a 200-minute period, respectively, for different airflow rates across the evaporator. The temperatures represented here were measured by a single thermocouple located beside the thermistor that was used to control the operation of the cycle.

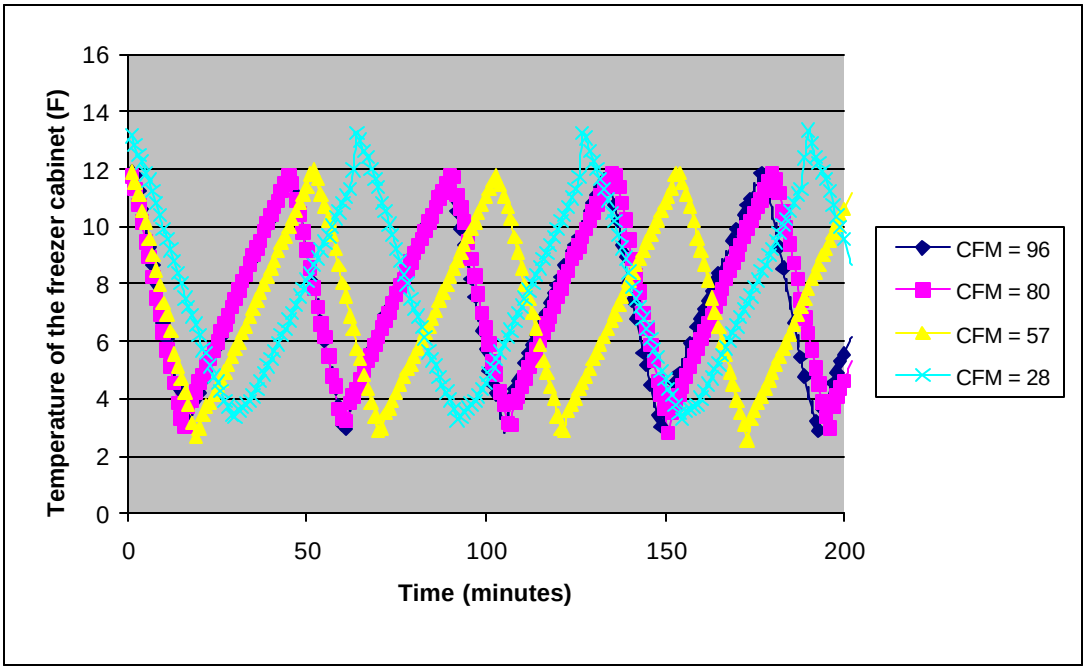

Figure 4.7 Temperature of the freezer cabinet as a function of time.

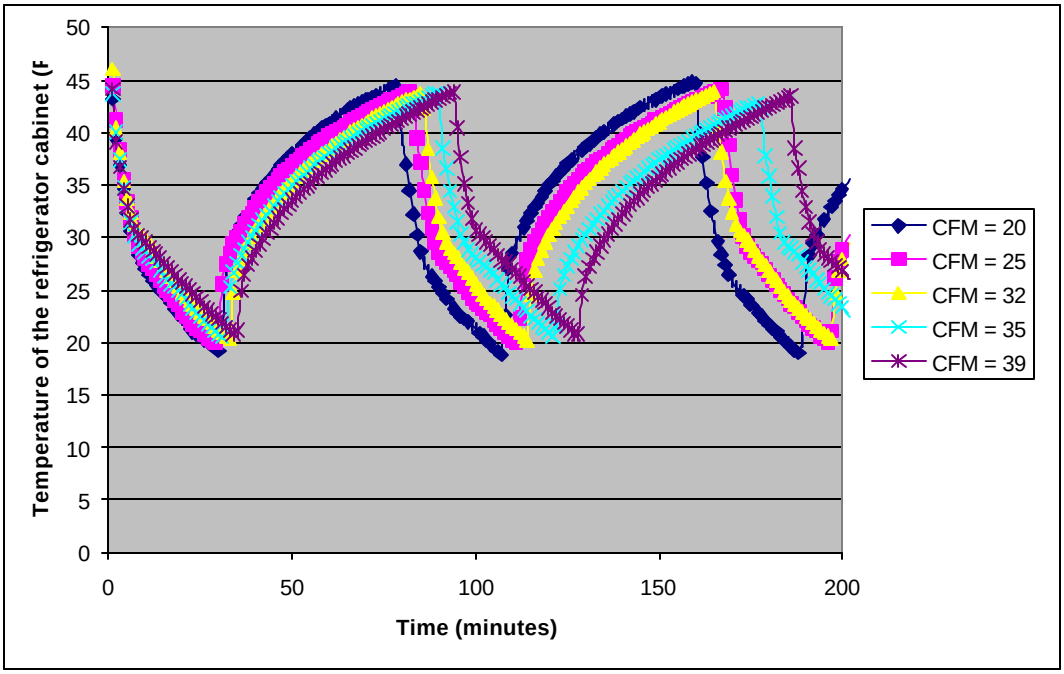

Figure 4.8 Temperature of the refrigerator cabinet as a function of time.

It can be seen that cabinet temperatures were essentially the same over a wide range of airflow rates, for the exception of the lowest airflow for the freezer. The fact that the average temperature over time was almost similar for all airflow rates over the range studied was an indication that the cabinet load did not differ significantly. Hence, this observation could not be used to explain the dependence of the load on the airflow rate.

As a consequence of its operation, the fan converts a portion of the electrical energy that it draws to heat. The higher degree of heat rejection by the fan for higher airflow rate flows was definitely a factor that contributed to the increase in cabinet load. However, the increase in fan heat rejection would only account for 1% out of the 18% increase (comparing lowest and highest airflow rate) in cabinet load even if all the extra electrical energy were converted to heat. Therefore, this explanation alone was not able to account for the increase in load with airflow rate.

Although not measured, the amount of stratification in the cabinet could have been a factor. While a higher degree of stratification is achieved when the airflow rate is low, the change in the apparent cabinet load according to the amount of stratification is difficult to quantify. Since a large stratification allows the temperatures to vary at different locations around the cabinet, an integral of the temperatures across the entire cabinet may reveal that it was actually kept at a higher temperature, resulting in a lower load. This is perhaps the best reason that explains the dependence of the cabinet load on the airflow rate.

4.3.2 Comparison with other Measurements

To demonstrate that they could meet the performance of the current heat exchanger at a lower cost, a leading manufacturer of heat exchangers had offered to measure the UA of the freezer evaporator. The measurements, which were performed by exchanging heat from air to water, are shown in Figure 4.9.

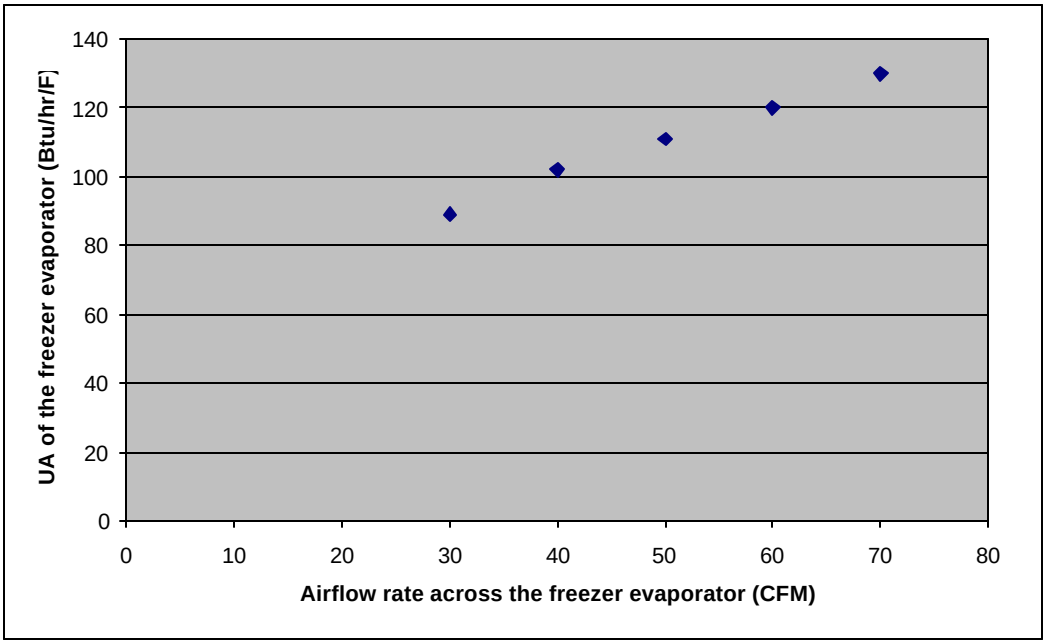

Figure 4.9 Measurements of the UA as a function of the airflow rate made by the heat exchanger manufacturer (used with permission from Sub-Zero Freezer Company).

A comparison between the UA curve for the freezer evaporator in Figure 4.1 and that from the manufacturer reveals that the former was consistently lower. The differences between the two sets of measurements can be explained as follows.

Owing to its transient nature, the UA increases with time even though the cooling capacity decreases as the evaporating temperature is lowered, as Figure 2.14 shows.

This behavior is observed because the log mean temperature difference decreases at a faster rate than the capacity. Since the UA in Figure 4.1 represents the value averaged over a cycle, it would increase if the cycle time were longer. For this reason, the UA will be higher if the cooling cycle was allowed to continue over a longer period until steady-state was approached, which was what the manufacturer did.

Moreover, the results by the manufacturer represent air-water UAs, whereas the UA curve in Figure 4.1 was obtained by refrigerant R134a to air measurements. This is likely to cause a difference because the UA depends on the heat transfer coefficient of both fluids that participate in this process. The extent to which the UA is affected by the fluids may be evaluated using Eqn. 3.2. However, this difference is unlikely to result in much change since most of the resistance to heat transfer is usually encountered in the air side and not the refrigerant or water that it communicates with.

4.3.3 Impact on Energy Consumption

The study on the UA would be incomplete without a discussion of its effect on the performance of the unit. This is because a larger UA is not necessarily accompanied by an increase in performance, as the case might be if the heat exchanger is already oversized. Tables 4.1-4.5 tabulate the energy consumption of the compressor and the fan for different airflow rates in the evaporators and condenser. Using Eqn. 4.2, the compressor and fan energies were calculated from the energy consumption per cycle and the on and off-cycle times, which were quantities that were measured from the experiment, as follows.

$$Energy/day = Energy/Cycle \times \left(\frac{\#Cycles}{Day} \right) \quad \text{Eqn. 4.2}$$

where $$\frac{\#Cycles}{Day} = \left(\frac{1440}{OnCycleTime + OffCycleTime} \right) \quad \text{Eqn. 4.3}$$

with the on and off-cycle times expressed in minutes. The energy/cycle was obtained by taking an average (of the compressor and fan energy consumption per cycle) over many cycles during the 20-hour testing period. Only cycles that were not running simultaneously were considered for this average since the power drawn would be different if the refrigerator and freezer cycles coincided. Hence, the compressor energy in Tables 4.1- 4.5 represents the predicted theoretical value calculated from experimental data if the cycles were to run separately throughout an entire test.

There are a few reasons why this approach was adopted in favor of summing the energy consumption over the testing period. Firstly, the refrigerator and freezer cycles had frequently coincide, causing the effect of running the cycles simultaneously to be confounded with the effect that the different fan speeds had on the performance of the system. By only using cycles that were running separately as explained above, the effect of different fan speeds could be studied independently. Secondly, defrosting often takes place sometime during the test period. Not only is the effect of defrosting on the total energy consumption significant, it would also be incorrect to subtract the energy consumed during the defrost process since the cabinet is warmed up when this process takes place.

Condenser fan speed (CFM)	Frez evap fan speed (CFM)	Frez on-cycle time (minutes)	Frez off-cycle time (minutes)	Frez energy consumption (Wh/cycle)	Freezer energy consumption (kWh/day)		
					Compressor	Fan	Total
124	96	17	27	45.6	1.329	0.163	1.492
124	80	17	27	44.2	1.296	0.149	1.445
124	57	21	30	52.2	1.327	0.146	1.473
124	28	30	33	67.6	1.399	0.146	1.545

Table 4.1 Freezer on and off-cycle times, and compressor and fan energy consumption for different evaporator fan speeds.

Condenser fan speed (CFM)	Refg evap fan speed (CFM)	Refg on-cycle time (minutes)	Refg off-cycle time (minutes)	Refg energy consumption (Wh/cycle)	Refrigerator energy consumption (kWh/day)		
					Compressor	Fan	Total
124	39	34	55	57.3	0.794	0.133	0.927
124	35	32	55	55.1	0.789	0.123	0.912
124	32	31	52	52.9	0.805	0.114	0.919
124	25	27	49	44.8	0.747	0.101	0.848
124	20	30	52	46.8	0.724	0.097	0.821

Table 4.2 Refrigerator on and off-cycle times, and compressor and fan energy consumption for different evaporator fan speeds.

Frez evap fan speed (CFM)	Condenser fan speed (CFM)	Frez on-cycle time (minutes)	Frez off-cycle time (minutes)	Frez energy consumption (Wh/cycle)	Freezer energy consumption (kWh/day)		
					Compressor	Fan	Total
57	152	21	30	52.7	1.310	0.177	1.487
57	131	21	30	53.0	1.347	0.148	1.495
57	124 **	21	30	52.2	1.321	0.144	1.466
57	107	21	30	51.9	1.327	0.139	1.466
57	62	21	30	53.0	1.369	0.126	1.496
57	0	*	*	*	Over 2	*	*

Table 4.3 Freezer on and off-cycle times, and compressor and fan energy consumption for different condenser fan speeds.

Refg evap fan speed (CFM)	Condenser fan speed (CFM)	Refg on-cycle time (minutes)	Refg off-cycle time (minutes)	Refg energy consumption (Wh/cycle)	Refrigerator energy consumption (kWh/day)		
					Compressor	Fan	Total
25	152	27	47	44.4	0.733	0.131	0.864
25	131	27	49	45.1	0.729	0.125	0.854
25	124 **	27	49	44.8	0.747	0.101	0.848
25	107	27	49	44.1	0.742	0.095	0.837
25	62	27	50	45.1	0.761	0.082	0.843
25	0	*	*	*	Over 1	*	*

Table 4.4 Refrigerator on and off-cycle times, and compressor and fan energy consumption for different condenser fan speeds.

Condenser fan speed (CFM)	Refrigerator energy (kWh/day)			Freezer energy (kWh/day)			Grand total (kWh/day)
	Compressor	Fan	Refg total	Compressor	Fan	Frez total	
152	0.733	0.131	0.864	1.310	0.177	1.487	2.351
131	0.729	0.125	0.854	1.347	0.148	1.495	2.349
124	0.747	0.101	0.848	1.321	0.144	1.466	2.314
107	0.742	0.095	0.837	1.327	0.139	1.466	2.303
62	0.761	0.082	0.843	1.369	0.126	1.496	2.339
0	Over 1	*	*	Over 2	*	*	Over 3

Table 4.5 The compressor, fan and total energy consumption for the freezer and refrigerator for different condenser fan speeds.

* Greatly depends on whether the cycles run simultaneously.
** The current airflow is 124 CFM for the case without any grill, which was the way the measurements were made.

The results in Table 4.1 suggest some room for improvement for the freezer evaporator. By increasing the airflow to 80 CFM, a decrease of 2% in energy consumption can be realized. Despite of a higher cabinet load, the increase in airflow rate had sufficiently enhanced the system performance to produce a net saving in energy consumption. This is because the increase in evaporator UA was successful in elevating the evaporating saturation temperature, which greatly influences the performance of a cycle.

An increase in the condenser UA does not lead to a similar outcome. The decrease in compressor power is not justified by the larger power that the fan draws. Even the refrigerator cycle, which carries a larger condenser load, does not appear to benefit from the higher airflow. Not only does this indicate that the condenser is accurately sized, but it also reinforces the fact that the performance of the system is more sensitive to the evaporating than condensing temperatures.

System performance is not always enhanced or insensitive to the increase in the fan speed. Such is the case for the refrigerator evaporator. A higher fan speed decreases the level of stratification in the cabinet and discharges a larger amount of heat into the cabinet, which ultimately leads to a higher cabinet load. Since the evaporator was already oversized, the increase in airflow was unable to raise the evaporating temperature and improve the performance of the cycle. Besides the increase in the compressor energy consumption, the fan also consumes more energy at higher speeds. It follows then, that the total energy consumption of the fan and compressor increases with the airflow rate.

4.4 Conclusions

The present freezer evaporator seems to be undersized. Experimental results have demonstrated that a 40% increase in the airflow rate was accompanied by a 2% energy saving. On the other hand, no improvement can be expected by running the condenser and refrigerator evaporator fans at higher speeds, which suggest that they are operating in the vicinity of their optimum points. In fact, a small improvement is possible by reducing the speed of the refrigerator evaporator fan to conserve energy. Alternatively, a smaller evaporator for the refrigerator could be installed with reduced cost without compromising its performance.

While the more accurate sizing of heat exchangers can only contribute a 2% improvement, a larger portion of the energy savings lies in the advantages that the more efficient DC fans can offer. In all, the use of the DC fans yields a 6% savings for the freezer and a further 2.8% for the refrigerator. Hence, the replacement of the existing AC fans with those tested in this experiment remains the most promising option in saving energy.

CHAPTER 5 Suction-Line Heat Exchangers

5.1 Introduction

Suction-line, or liquid suction heat exchangers, are commonly installed in small halocarbon refrigeration systems. The primary objective of this device is to improve the performance of the cycle by increasing the refrigeration effect. Figure 5.1 illustrates the location of a suction-line heat exchanger in a vapor-compression cycle while Figure 5.2 shows the physical location of this heat exchanger in this refrigerator.

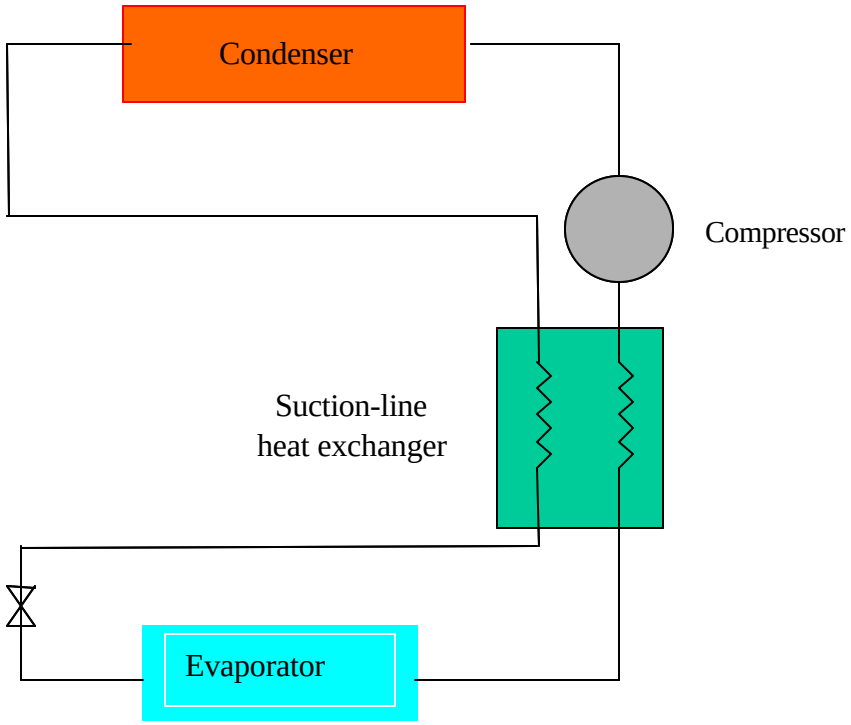

Figure 5.1 Schematic identifying the location of a suction-line heat exchanger.

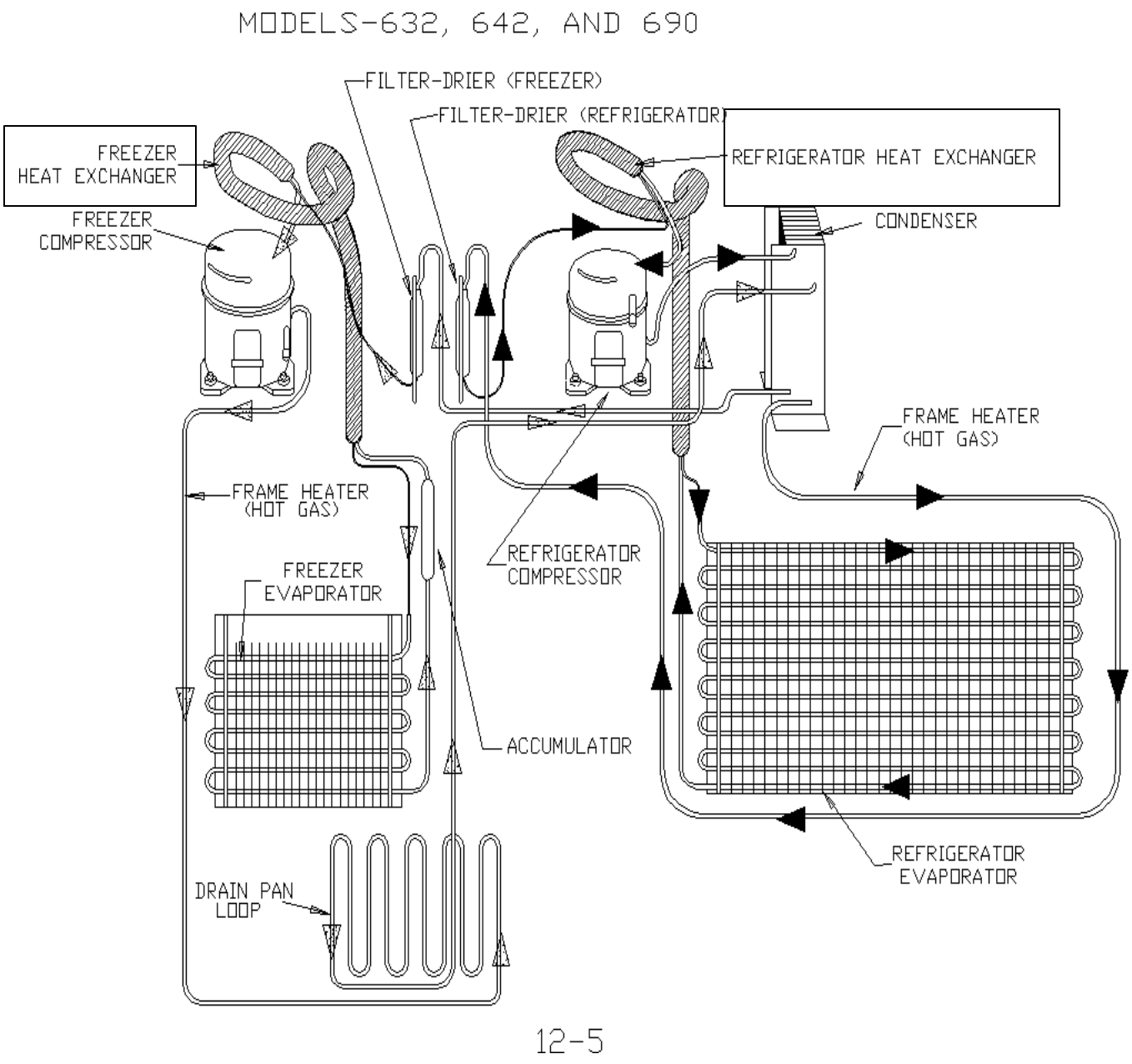

Figure 5.2 Refrigeration schematic showing the major components including a suction-line heat exchanger (Courtesy of Sub-Zero Freezer Co.)

5.2 Advantages and Disadvantages of Suction-Line Heat Exchangers

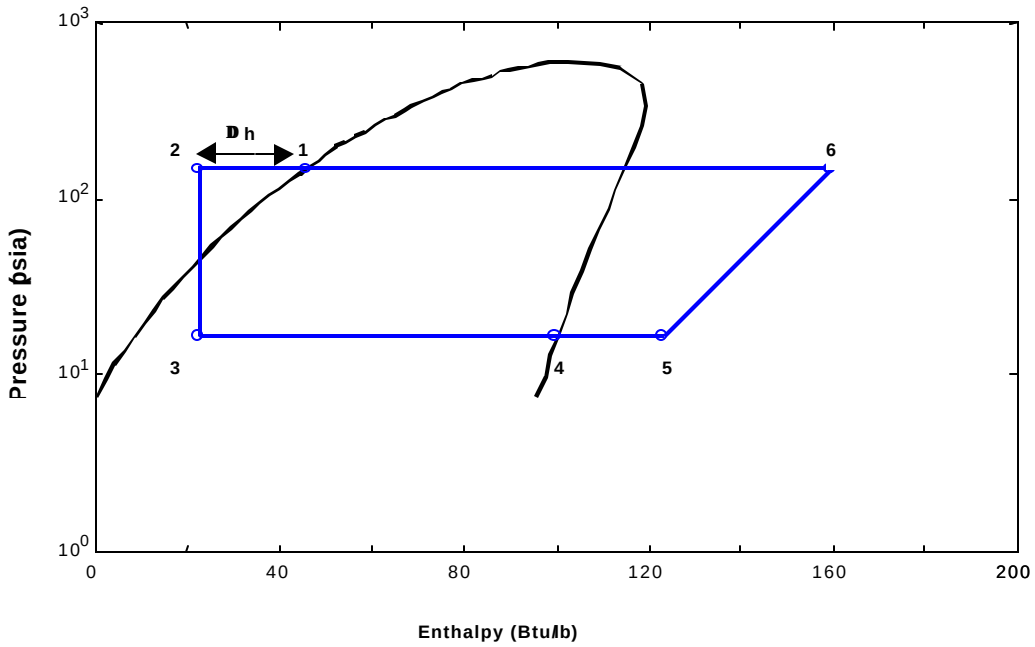

Figure 5.3 Property plot for R134a showing the benefits of subcooling.

To increase the effect of refrigeration, the liquid refrigerant that exits the condenser is subcooled before it is throttled through the expansion device. By reducing the temperature and the enthalpy of the incoming two-phase refrigerant, the difference between the enthalpy of the refrigerant across the evaporator is increased by the amount (Δh) shown on the P-h diagram in Figure 5.3. If no other effects were present, the cooling of the refrigerant would increase the refrigeration capacity of the cycle since it is proportional to this enthalpy difference.

Subcooling the liquid refrigerant also ensures that any residual vapor from the condenser is removed prior to its entry into the capillary tube. This is an added advantage since any formation of flash gas at the inlet of the expansion device will affect its ability to

function properly. This is because the vapor, which has a large specific volume, will interfere with the flow of liquid into the capillary tube. In the absence of the suction-line heat exchanger, the system will equilibrate at a higher condensing pressure to condense any flash gas that forms, and by doing so, the burden on the compressor is increased.

The source of subcooling for the liquid is provided by low temperature vapor leaving the evaporator. The energy removed from cooling the saturated liquid also ensures removal of any residual liquid refrigerant leaving the evaporator. This effect is especially important since the presence of two-phase refrigerant is detrimental to the compressor.

However, this advantage is moderated by the fact that the vapor enters the compressor at a higher temperature than it would without the suction-line heat exchanger. Since compressors have a fixed rate of displacement, an increase in the temperature of the suction gas decreases the density of the gas and leads to a reduction in the mass flow and hence, the refrigeration capacity.

Apart from the increased temperature of the suction gas, the suction-line heat exchanger adds a pressure drop on the low-side which adversely affects the performance of the cycle. This is because a pressure drop will reduce the gas density at the suction line, and consequently, the mass flow rate. Besides this, the decrease in pressure on the low-side also forces the compressor to operate over a larger pressure ratio, resulting in an increased in power consumption per unit mass.

It is clear that suction-line heat exchangers produce two competing effects. For these heat exchangers to be effective, the increase in the evaporator enthalpy difference should overweigh the reduction in mass flow and the increased pressure ratio so that the combined effect results in an increase in both capacity and COP.

5.3 Suction-Line Heat Exchangers in this Refrigerator

The ability of a suction-line heat exchanger to transfer heat between the warm liquid and the cool gas is characterized by its effectiveness, which is expressed as follows

$$e = \frac{(T_5 - T_4)}{(T_1 - T_4)} \qquad \text{Eqn. 5.1}$$

where the subscripts refer to the states of the refrigerant in Figure 5.3. The effectiveness of this device depends, in part, on the surface area available for heat transfer. A larger area of contact will promote the heat transfer process; thereby, increasing the effectiveness. Figure 5.4 shows the arrangement of this heat exchanger in this refrigerator.

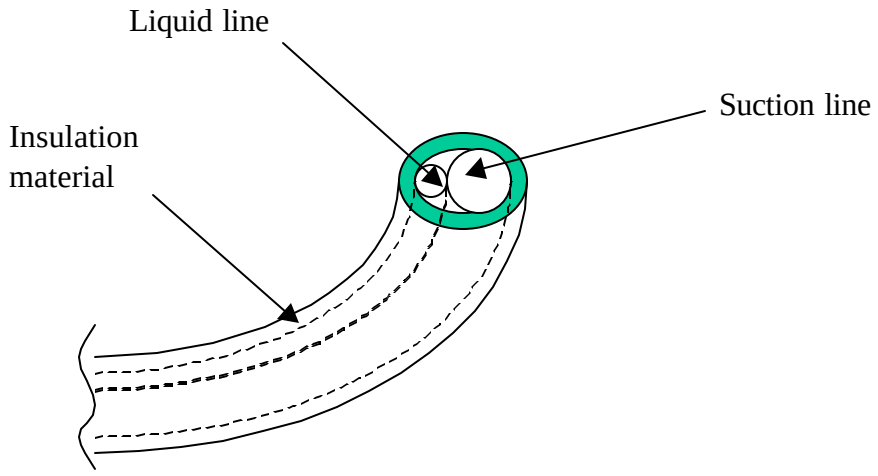

Figure 5.4 A diagram of a suction-line heat exchanger.

In both the freezer and the refrigerator, the length of the suction-line heat exchangers is 6 ft while the inner diameters of the liquid line and suction line are 0.125 in and 0.276 in,

respectively. The tubes, which are soldered together, are insulated to ensure that very little heat is gained from the surroundings. In addition, this heat exchanger is typically very long so that the area of contact is increased. As crude as this configuration may seem, it provides a very efficient mode for heat exchange between the two streams in contact (the effectiveness of the suction-line heat exchangers in this refrigerator exceed 90%). The advantages and disadvantages of suction-line heat exchangers are studied in greater detail below. In particular, the impact of a higher temperature suction vapor, temperature lift and pressure drops will be analyzed, in that order.

5.4 Effects of High Temperature Vapor

In this analysis, saturated conditions are assumed for the refrigerant at the exit of the evaporator and condenser. Although typical refrigerator compressors do not behave in an adiabatic fashion, the heat rejection from the surface of the compressor was neglected. In addition, the suction-line heat exchanger was assumed to be adiabatic and any low-side pressure drop across this device was neglected. A pressure drop was not considered here to enable a study on the impact of high temperature vapor alone. For the exception of the pressure drop (which will be studied later), the above assumptions are either quite accurate or do not have a significant impact on the analysis. The performance of the compressor was

characterized using an isentropic efficiency. Even though the value of this parameter was assumed, it was found to have no bearing on the conclusions drawn from this study.

As Figure 5.3 shows, suction-line heat exchangers increase the refrigerating capacity per unit mass by the difference between the enthalpy of the refrigerant at states 1 and 2. If the change in suction gas temperature was assumed to have no effect on the mass flow rate, then an increase in the effect of refrigeration is expected; however, the superheating of the suction vapor by the liquid increases the specific volume of the gas entering the compressor. With the specific volume being inversely proportional to the density, the amount of mass that the compressor pumps per unit time will decrease, as Eqns. 5.2 and 5.3 (Threlkeld, 1962) show.

$$\dot{m} = \frac{h_{vol} PD}{v_{enter,comp}} \qquad \text{Eqn. 5.2}$$

and $$h_{vol} = \left[1 + C - C\left(\frac{P_{con}}{P_{evap}} \right)^{\frac{1}{n}} \right] \times \left(\frac{v_{enter,comp}}{v_{suction}} \right) \qquad \text{Eqn. 5.3}$$

where h_{vol} = volumetric efficiency
C = clearance volume
PD = displacement rate of the piston
n = polytropic exponent
$n_{enter,comp}$ = volume of the refrigerant entering the compressor
$n_{suction}$ = volume of the refrigerant at the suction-line

For this analysis, no pressure drops or additional heating of the vapor in the intake line of the compressor was considered. Hence, the condition of the gas entering the compressor (from the suction-line heat exchanger) is similar to that at the suction-line. Combining Eqns. 5.2 and 5.3, the mass flow rate may be rewritten as follows.

$$\dot{m} = \left[1 + C - C\left(\frac{P_{con}}{P_{evap}}\right)^{\frac{1}{n}}\right] \times \left(\frac{PD}{v_{suction}}\right) \qquad \text{Eqn 5.4}$$

and the capacity as

$$Capacity = \left[1 + C - C\left(\frac{P_{con}}{P_{evap}}\right)^{\frac{1}{n}}\right] \times \left(\frac{PD}{v_{suction}}\right) \times \left(h_4 - h_3\right) \qquad \text{Eqn. 5.5}$$

where the subscripts correspond to the states of the refrigerant in Figure 5.3. For a compressor, the clearance volume and the rate of displacement are fixed and not functions of the suction conditions. Similarly, the evaporating and condensing temperatures only depend on the cabinet and ambient temperatures as well as the sizes of the evaporator and condenser. Therefore, the only parameters that affect the capacity are h_3 and $n_{suction}$. Figure 5.5 plots the change in mass flow rate as a function of the heat exchanger effectiveness while the combined effects of h_3 (which affects the refrigeration capacity) and $n_{suction}$ (determines the refrigerant mass flow) on the capacity are illustrated in Figure 5.6.

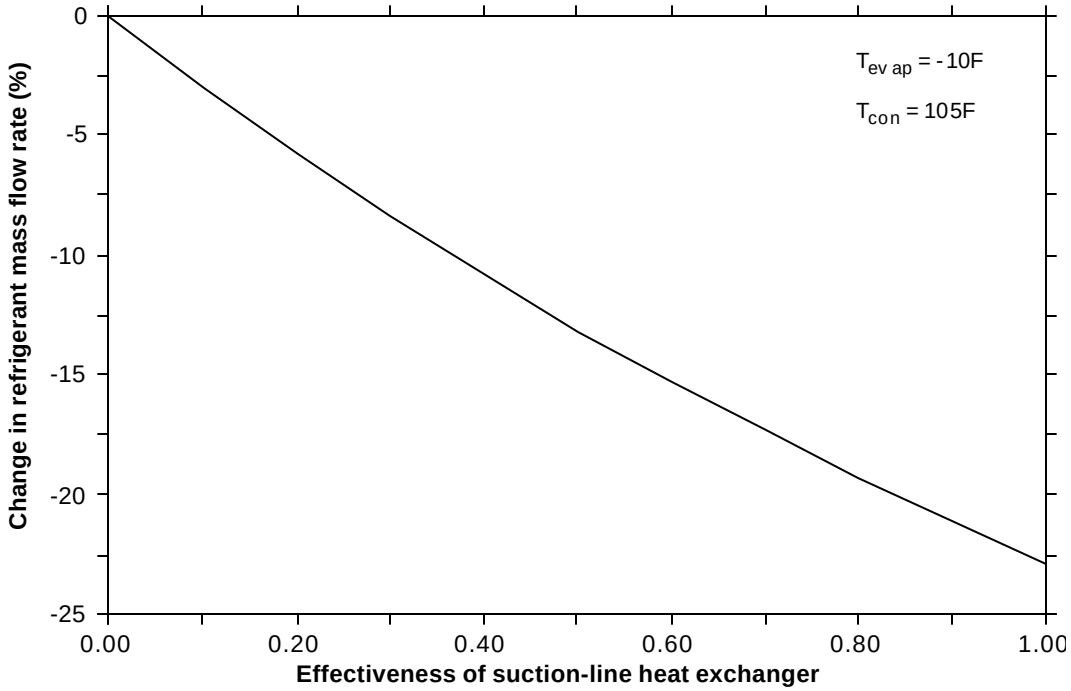

Figure 5.5 The impact of the suction-line heat exchanger effectiveness on the mass flow rate for cycles using R134a.

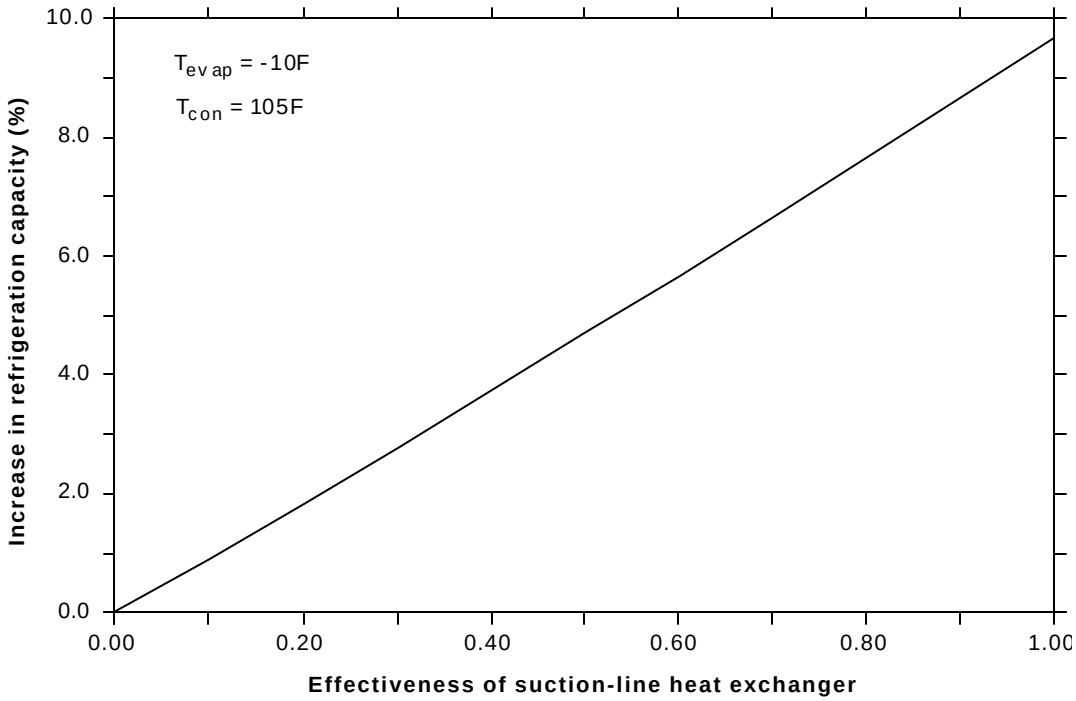

Figure 5.6 The impact of the suction-line heat exchanger effectiveness on the capacity for cycles using R134a.

Figure 5.5 shows that the rate of mass flow decreases with heat exchanger effectiveness for cycles using R134a. The sole factor responsible for this downward trend was the decrease of the suction gas density. Despite of a smaller mass flow, Figure 5.6 shows that the cycle had still experienced a net increase in capacity. Clearly, the effect of subcooling was greater than the reduction in mass flow for this refrigerant. Specifically, the capacity of cycles using R134a had increased by 9.6% (difference between effectiveness of 0 and 1) for this combination of evaporating and condensing temperatures.

Apart from the capacity, the power drawn by the compressor is also of importance. An analysis by Threlkeld (1962) yields the following expression for the work done per unit mass by the compressor.

$$w = \frac{n}{(n-1)} P_{evap} v_{suction} \left[\left(\frac{P_{con}}{P_{evap}} \right)^{\frac{n-1}{n}} - 1 \right] \qquad \text{Eqn. 5.6}$$

The power consumed by the compressor depends on the efficiency of the motor, hence

$$\dot{W} = \frac{\dot{m} w}{h_{motor}} \qquad \text{Eqn. 5.7}$$

$$= \frac{n P_{evap}}{(n-1)} \left[\left(\frac{P_{con}}{P_{evap}} \right)^{\frac{n-1}{n}} - 1 \right] \times \frac{h_{vol} PD}{h_{motor}} \qquad \text{Eqn. 5.8}$$

As Eqn. 5.8 shows, the heat exchanger does not affect the compressor power since all parameters are independent of the suction vapor. Because the COP is the ratio of the capacity to the power, it will assume an identical trend as the capacity.

Suction-line heat exchangers were shown to be suitable for systems employing R134a as it produced a maximum of 9.6% boost in performance. Despite of the lower mass flow, the effect of subcooling was able to produce a net increase in the capacity of the cycle. With the decrease in mass flow having no effect on the compressor power, the COP will increase by the same amount as the capacity. This maximum increase of 9.6% only applies for the evaporating and condensing temperatures assumed earlier. The effect of temperature lift on this increase is the subject of the following discussion.

5.5 Effect of Temperature Lift

Refrigerator and freezer cabinets are kept at different temperatures. In systems where cooling is provided by two separate cycles, the freezer compressor is forced to operate over a larger pressure ratio than the refrigerator. Such is the case with this side-by side unit. Since the refrigerator cabinet is on the order of 30°F higher than the freezer, the temperature lift is significantly lower. Consequently, it is important to study whether the advantages which suction-line heat exchangers offer to the freezer cycle apply for cycles operating at other evaporating temperatures.

The change in capacity for cycles with different temperature lifts is shown below. To study the effect of temperature lifts alone, pressure drops in the heat exchangers were neglected.

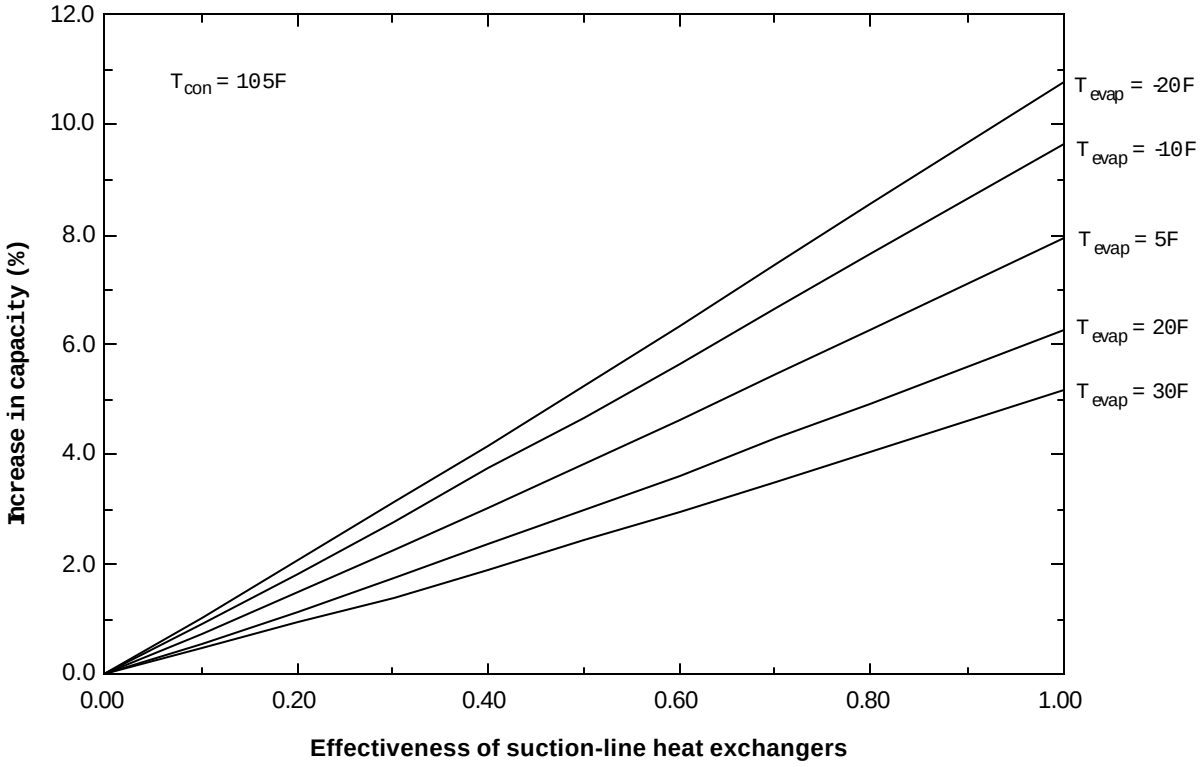

Figure 5.7 The effect of suction-line heat exchanger effectiveness on capacity for cycles with different temperature lifts. All cycles use R134a.

Figure 5.7 clearly shows that the benefit of subcooling was more pronounced when the temperature lift was greater. The improvement in performance ranged from 5.2% for the cycle with the lowest temperature lift (pressure ratio of 3.7) to 10.8% for the cycle with the largest lift (pressure ratio of 11.6). In particular, the refrigerator and freezer cycles with evaporating temperatures of 20°F and –10°F realized a 5.8% and 8.7% gain in capacity, respectively (based on an effectiveness of 0.9 in both cycles).

The larger increase in the refrigeration effect for cycles with lower evaporating temperatures can be explained by Figure 5.8.

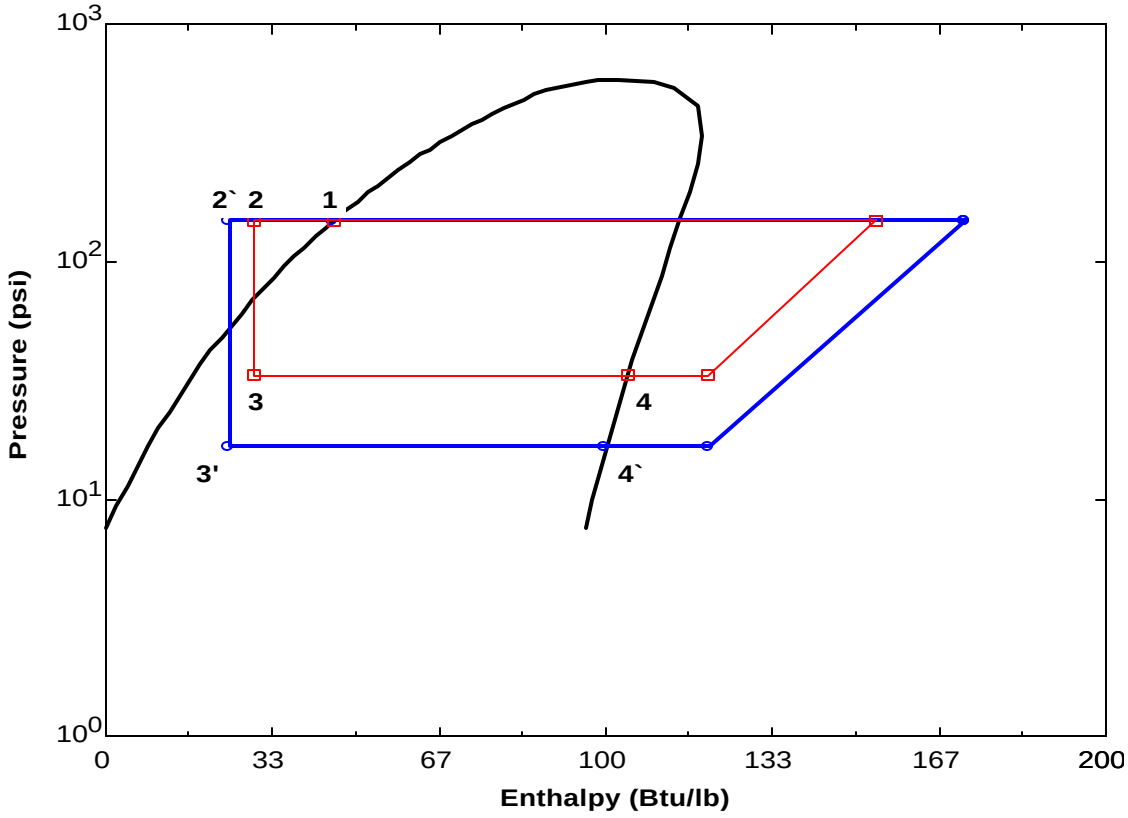

Figure 5.8 Property plot showing the states of the refrigerant for two cycles with different temperature lifts.

Referring to Figure 5.8, the percentage increase in capacity per unit mass for both cycles may be expressed as

$$\Delta Capacity_{higher,evap,temp} \propto \frac{h_1 - h_3}{h_4 - h_1} \qquad \text{Eqn. 5.9}$$

$$\Delta Capacity_{lower,evap,temp} \propto \frac{h_1 - h_{3`}}{h_{4`} - h_{1`}} \qquad \text{Eqn. 5.10}$$

With $h_3 > h_{3`}$ and $h_4 > h_{4`}$, the potential for an increase in capacity is clearly larger for the expression in Eqn 5.10. Unfortunately, the effects of a decrease in mass flow rate is also more significant for low evaporating temperature cycles. This is because the vapor has to undergo a larger temperature rise in the suction-line heat exchanger (the vapor enters the heat exchanger at a lower temperature for cycles with lower evaporating temperatures but they all exit at the same temperature), which results in a higher degree of superheating. Because the increase in the refrigeration effect is greater than the decrease in mass flow, the net effect is a larger increase in capacity for cycles with lower evaporating temperatures for R134a.

5.6 Effect of Low-Side Pressure Drop

In Section 5.4, the mass was corrected for higher temperature gas entering the compressor. Any pressure drop that resulted from friction against the walls of the suction-line heat exchanger was neglected. In reality, however, a fluid will always experiences some shear stress, which ultimately leads to a loss in fluid pressure. The extent of this pressure drop depends, among others, on the length and the number of bends in the tubes carrying the refrigerant and may be determined by Eqn. 5.11.

$$\Delta P = \left(\frac{fL}{D} + K \right) \times \frac{r V^2}{2} \qquad \text{Eqn. 5.11}$$

with $f = \left(\frac{64}{\mathrm{Re}_D} \right)$ for laminar flow Eqn. 5.12

or $\frac{1}{\sqrt{f}} = -1.8 \log_{10} \left[\frac{6.9}{Re_D} + \left(\frac{\varepsilon_{rough}}{3.7D} \right)^{1.11} \right]$ for turbulent flow (Haaland, 1983) Eqn. 5.13

where f = friction factor
K = loss coefficient
e_{rough} = relative roughness of the pipe

The loss coefficient in Eqn. 5.11 is a measure of the loss in pressure that results when the refrigerant encounters any valves, bends in the pipes or sudden expansions. The length and inside diameter of the suction tube was approximately 6 ft and 0.276 in, respectively. Since the tube was mainly straight with a few bends near the compressor, the loss coefficient was assumed to be 0.5, which corresponds to five 90° bends (White, 1986). For tubes that are drawn, the relative roughness is estimated to be 0.000005 in. Using these values and a mass flow rate of 8.6 lb_m/hr for the freezer, the flow was determined to be turbulent with a Reynolds number of 17632 while the pressure drop was calculated to be 0.09 psi. With a mass flow of 7.2 lb_m/hr, the Reynolds number was 14762, resulting in a 0.06 psi drop in pressure for the refrigerator. The pressure drop affects the system in two ways.

5.6.1 Effects of Lower Mass Flow

Like the effect of high temperature gas on the mass pumped by the compressor, a lower pressure decreases the density of the superheated vapor entering the compressor. Referring to Eqn. 5.5, the capacity is inversely proportional to the specific volume of the

suction gas. With the remaining parameters unchanged, a pressure drop will result in a higher specific volume and thus, a lower capacity. The same, however, is not true for the power consumption. Eqn. 5.8 shows that the power is essentially independent of suction gas volume. For a fixed compressor using a particular refrigerant, the only parameters that affects the power are the evaporating and condensing pressures. Hence, the increase in the specific volume of the suction vapor reduces the capacity but has no impact on the power that the compressor draws.

5.6.2 Effects of a Higher Pressure Ratio

When the vapor loses pressure prior to its entry into the compressor, the suction pressure is reduced. By increasing the pressure ratio that the compressor has to operate over, the power *per unit mass* that is consumes increases. However, the impact of this larger pressure ratio is less than the effect of the decrease in mass flow that results from the increased suction volume. Consequently, the power drawn by the system decreases when the vapor enters the compressor at a lower pressure. Rearranging Eqn. 5.8, the compressor power consumption is proportional to the evaporating pressure raise to the power of $1/n$, which is consistent with the observation that the power decreases when a pressure drop is present.

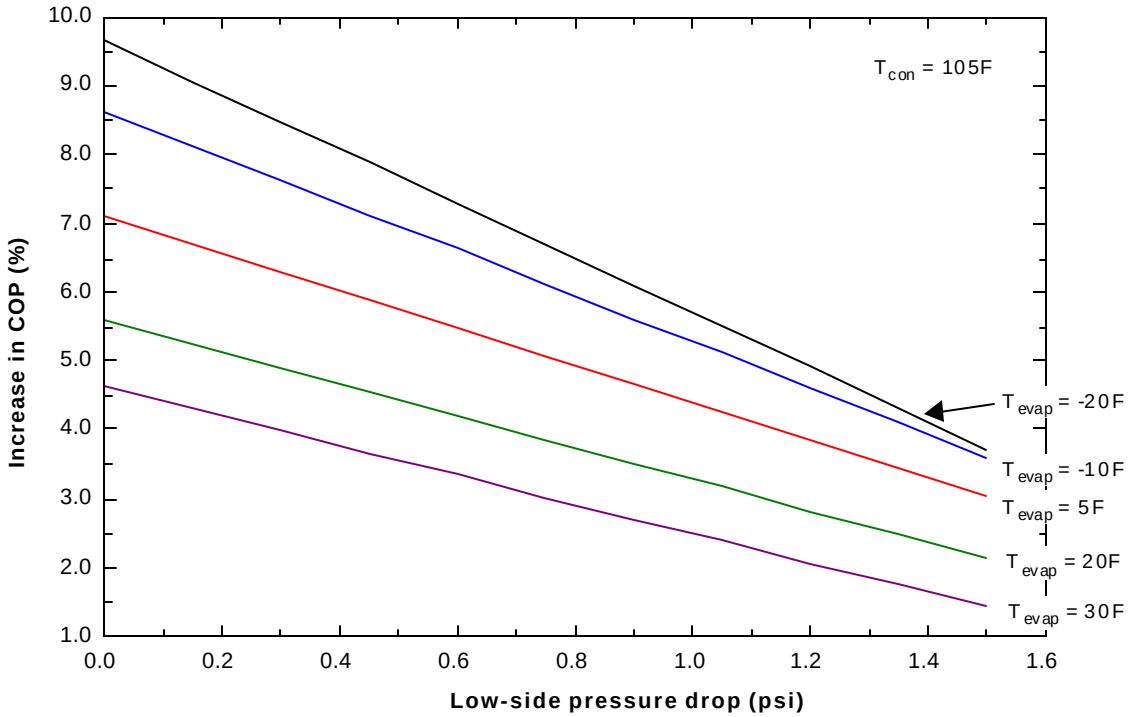

Figure 5.9 The effect of low-side pressure drop on the increase in capacity for five cycles with different temperature lifts. A suction-line heat exchanger effectiveness of 0.9 was assumed for all cycles.

Therefore, the drop in low-side pressure creates two opposing effects on the COP. With both the capacity and power decreasing simultaneously, the net effect on the COP depends on the rate at which these two parameters decrease as a function of the pressure drop and will be studied in detail below.

Figure 5.9 shows that the performance of all cycles decrease with pressure drop in a linear fashion. The degree of sensitivity to the pressure drop is seen to be a function of temperature lift. Just as the cycles with the highest temperature lift had benefited most from suction-line heat exchangers, they also pay the greatest price for any pressure drops on the low-side. With a 0.1 psi drop in pressure estimated earlier, the freezer and the refrigerator cycles would experience a 8.3% and 5.4% increase in performance respcetively. For the refrigerator, which has an evaporating temperature of 20°F, the capacity decreases by

approximately 2% for every 1 psi drop in pressure. The freezer (-10°F), on the other hand, was more sensitive to the changes with an average decrease of 3% for every 1 psi drop in suction pressure.

5.6.3 "Allowable" Pressure Drop

There seems to be an "allowable" pressure drop, which is defined as the maximum pressure drop that is permitted in a cycle before it losses all the benefits obtained from liquid subcooling. Figure 5.10 shows this "allowable" pressure drop for cycles that use R134a.

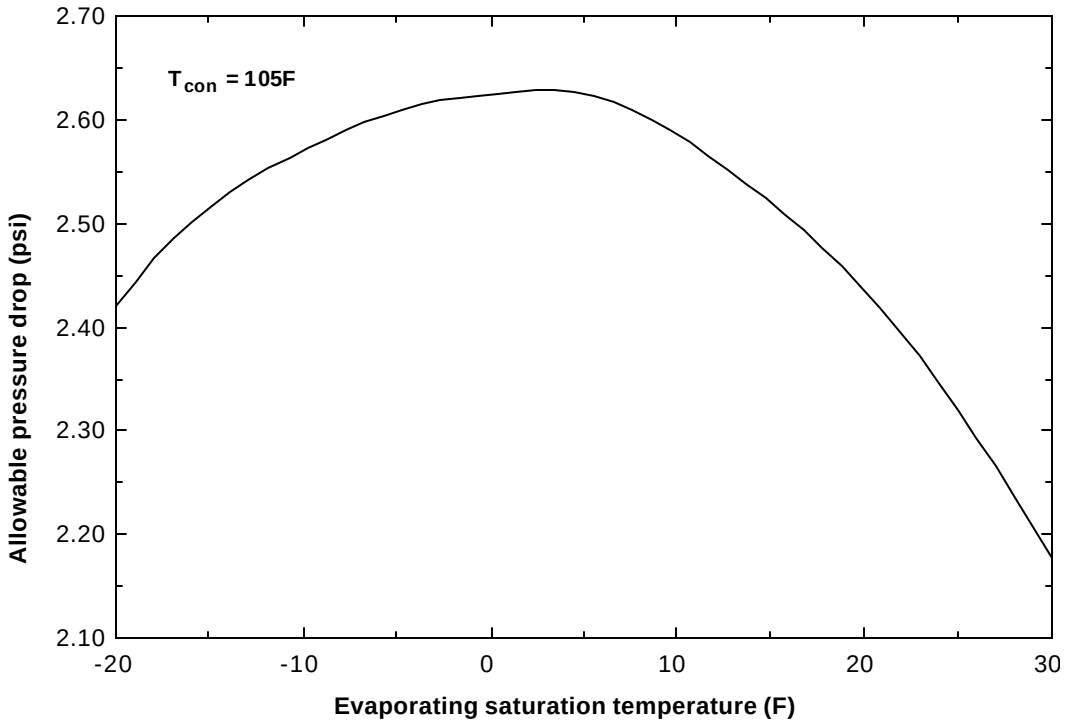

Figure 5.10 The allowable pressure drop for different evaporating temperatures. The suction-line heat exchangers have an effectiveness of 0.9.

For the range of temperatures studied, the allowable pressure was highest for cycles with evaporating temperatures of 0-5°F. For all cycles operating within the range of –20 to 30°F, the allowable pressure was greater than 2.1 psi, which is much larger than the estimated pressure drops in the current heat exchangers. The trend here can be explained as follows. It has been shown that cycles with larger temperature lifts had registered greater benefits from the use of suction-line heat exchangers. However, they were also found to be the most vulnerable to pressure drops in the system. The maximum in Figure 5.10 merely identifies the temperatures which had benefited the most from subcooling while paying the least for any pressure drops. To the right of this maximum, the benefits from subcooling were smaller and a lower pressure drop was seen to be sufficient in erasing all the advantages from the increased refrigeration effect. The opposite was true for cycles with evaporating temperatures that were lower than 0°F. Although cycles with low evaporating temperatures had demonstrated huge capacity increases from subcooling, the effects of pressure drops were also more pronounced so that all the gains from subcooling would be defeated at a lower pressure drop.

5.7 Conclusions

The use of suction-line heat exchangers in a vapor-compression cycle has been studied for the current refrigerator. An attempt to increase the refrigeration capacity by subcooling the liquid from the condenser was seen to produce two opposing effects. As a product of liquid subcooling, the suction vapor enters at a higher temperature than it would otherwise have. While the desired effect of liquid subcooling was achieved, the gain in refrigeration capacity was diminished by the decrease in the mass flow rate.

The benefits of installing a suction-line heat exchanger was also shown to be a function of the temperature lift of the cycle. Cycles operating over a larger pressure ratio were inherently more sensitive to the effectiveness of the heat exchanger, and had demonstrated a greater potential for an increase in COP.

Pressure drops on the low-side have been found to adversely affect the performance of the system. Not only does it require the compressor to operate over a larger pressure ratio, the decrease in suction pressure will also raise the specific volume of the suction vapor. While cycles with a larger temperture lift were seen to profit the most from suction-line heat exchangers, they were also found to be more vulnerable to any signs of pressure drop. Hence, where a significant pressure drop is expected, an analysis should be carried out to determine whether the desired effects of subcooling will ultimately be negated by the harmful effects that arise from low-side pressure drops.